Neuron, Vol. 47, 803–815, September 15, 2005, Copyright ©2005 by Elsevier Inc. DOI 10.1016/j.neuron.2005.08.023

GABAergic Excitation Promotes Neuronal Differentiation in Adult Hippocampal Progenitor Cells

Yusuke Tozuka,[1] Satoshi Fukuda,[1] Takashi Namba,[2] Tatsunori Seki,[2] and Tatsuhiro Hisatsune[1,*]
[1]Department of Integrated Biosciences
University of Tokyo
Kashiwa 277-8562
Japan
[2]Department of Anatomy
Juntendo University School of Medicine
Tokyo 113-8421
Japan

Summary

Hippocampal activity influences neurogenesis in the adult dentate gyrus; however, little is known about the involvement of the hippocampal circuitry in this process. In the subgranular zone of the adult dentate gyrus, neurogenesis involves a series of differentiation steps from radial glia-like stem/progenitor (type-1) cells, to transiently amplifying neuronal progenitor (type-2) cells, to postmitotic neurons. In this study, we conducted GFP-targeted recordings of progenitor cells in fresh hippocampal slices from nestin-GFP mice and found that neuronal progenitor (type-2) cells receive active direct neural inputs from the hippocampal circuitry. This input was GABAergic but not glutamatergic. The GABAergic inputs depolarized type-2 cells because of their elevated $[Cl^-]_i$. This excitation initiated an increase of $[Ca^{2+}]_i$ and the expression of NeuroD. A BrdU-pulse labeling study with $GABA_A$-R agonists demonstrated the promotion of neuronal differentiation via this GABAergic excitation. Thus, it appears that GABAergic inputs to hippocampal progenitor cells promote activity-dependent neuronal differentiation.

Introduction

Adult neurogenesis occurs in the dentate gyrus of the hippocampus (Altman and Das, 1965; Seki and Arai, 1991, 1993; Cameron et al., 1993; Eriksson et al., 1998; Kornack and Rakic, 1999; Palmer et al., 2000; van Praag et al., 2002), which may underpin the modulation of cognitive brain functions (Shors et al., 2001; Feng et al., 2001; Drapeau et al., 2003). Considerable evidence exists to support the concept that neural activity alters the rate of neurogenesis in this area (Cameron et al., 1995; Bengzon et al., 1997; Parent et al., 1997; Malberg et al., 2000; Blümcke et al., 2001; Nacher et al., 2001). Although this implies that neural inputs act directly on adult hippocampal progenitor cells, very little information exists regarding the neural connections between these cells and the hippocampal network. In order to understand the regulatory mechanism underlying neuronal differentiation, it is important to determine the types of neural inputs on adult hippocampal progenitor cells and their physiological effects.

In a previous study, we identified a two-step differentiation process in an early phase of adult neurogenesis (Fukuda et al., 2003), from radial glia-like stem/progenitor cell (type-1 cell) to transiently amplifying neuronal progenitor cell (type-2 cell). A similar finding has also been reported by other groups (Seri et al., 2001, 2004; Filippov et al., 2003; Kronenberg et al., 2003; Steiner et al., 2004). The characteristics of the type-1 cell resemble those of radial glial cells residing in the embryonic ventricular zone, which have recently been recognized as neural stem cells (Noctor et al., 2001; Miyata et al., 2001). The most notable characteristics of the type-2 cell are its extremely high input resistance (IR) and robust proliferative activity. Recently, a similar transiently amplifying neuronal cell type has also been reported in embryonic neocortex (Noctor et al., 2004). The unique properties of the type-2 cell led us to speculate that if neural inputs exist on these cells, they could provide the means to drive the genesis of new neurons.

This hypothesis that some activity-dependent regulation of neurogenesis is mediated through the progenitor cell is supported by reports demonstrating that in the developing brain, neurotransmitters such as GABA and glutamate can act to modulate the proliferation and differentiation of these cells (LoTurco et al., 1995; Antonopoulos et al., 1997; Haydar et al., 2000; Nguyen et al., 2003). It is well known that GABA acts as an inhibitory neurotransmitter in mature neurons; however, in immature cells, activation of $GABA_A$ receptors elicits a depolarization of the membrane potential because of the cells' increased E_{Cl} (Owens and Kriegstein, 2002; Ben-Ari, 2002). A pioneer study by Kriegstein and colleagues demonstrated that both GABA and glutamate depolarize embryonic cortical progenitor cells and then induce terminal differentiation for neurons (LoTurco et al., 1995). Therefore, it is reasonable to speculate that in the adult dentate gyrus, the release of both GABA and glutamate from the mature circuitry could have a regulatory effect on the neuronal differentiation of progenitor cells.

Depolarization of progenitor cells elicits an elevation of $[Ca^{2+}]_i$ through the activation of voltage-gated calcium channels, as previously reported for both embryonic and adult progenitor cells (LoTurco et al., 1995; Deisseroth et al., 2004). Very interestingly, Deisseroth et al. have demonstrated that this calcium signaling induced the expression of NeuroD, a positive regulator of neuronal differentiation. Indeed, NeuroD is required for differentiation of the granule cells in the dentate gyrus of the hippocampus (Liu et al., 2000), and its expression has been observed in differentiating adult dentate gyrus progenitor cells (Seki, 2002a, 2002b).

A major ascending fiber tract (perforant pathway) to the dentate gyrus originates from entorhinal cortex. These excitatory fibers make synapses with projecting granule neurons as well as local interneurons in the molecular layer of the dentate gyrus. Two subpopulations of hippocampal progenitor cells are found in the sub-

*Correspondence: hisatsune@k.u-tokyo.ac.jp

granular zone of the dentate gyrus. Type-1 cells extend their processes toward the molecular layer, whereas type-2 cells do not extend processes in any direction. It has also been reported that fibers from local interneurons ascend to the subgranular zone (Freund and Buzsaki, 1996; Mott et al., 1997). This finding suggests that progenitor cells could make contact with GABAergic and glutamatergic terminals from the surrounding hippocampal circuitry.

In this study, we used GFP-guided targeted-patch clump recording to investigate whether either type-1 or type-2 cells display functional expression of receptors for neurotransmitters such as GABA or glutamate. Our results demonstrate that type-2 cells receive excitatory GABAergic inputs but not glutamatergic inputs. This excitation increased $[Ca^{2+}]_i$ and induced the expression of NeuroD. The findings presented here provide evidence of GABAergic connections to dividing hippocampal progenitor cells, resulting in the activity-dependent promotion of neuronal differentiation in adult brain.

Results

Adult Hippocampal Transiently Amplifying Progenitor, Type-2, Cells Respond to GABA

We first investigated the types of neurotransmitter receptors found on type-1 and type-2 cells in the adult dentate gyrus by means of GFP-targeted-patch clump recording. For this purpose, we used nestin-GFP transgenic mice (Yamaguchi et al., 2000) in which GFP proteins are expressed under the control of the nestin promoter and its second intron (Zimmerman et al., 1994), allowing the expression of the transgene (GFP) in both cell types (Figure 1A). In fresh hippocampal slices from the nestin-GFP mice, we could easily detect a large number of GFP^+ cells within the subgranular zone (Figure 1B). Presumptive GFP^+ type-1 cells were initially identified microscopically by their radial glia-like processes (Figure 1C) and GFP^+ type-2 cells by their round soma and lack of visible processes (Figure 1D). After patching the cells, these two distinct subpopulations were confirmed based on their IR value (type-1 progenitor cells, IR < 0.5 GΩ; type-2 progenitor cells, IR > 0.5 GΩ).

We then investigated whether these progenitor cells respond to GABA, glutamate, or other authentic neurotransmitters. In the case of type-1 cells, we could not detect any currents after focal application of GABA (0%, n = 12), NMDA (0%, n = 11), AMPA (0%, n = 11), or glycine (0%, n = 11) (Figures 1E, 1F, 1G, and 1H, respectively). Surprisingly, however, we detected significant inward currents in most type-2 cells after the focal application of GABA (Figure 1I) (90.5%, n = 42). These GABA-evoked currents were completely and reversibly inhibited by bicuculline, a selective $GABA_A$ receptor ($GABA_A$-R) antagonist (100% of all GABA-responsive type-2 cells; n = 10), indicating that the responses were mediated by the activation of $GABA_A$-Rs. The dose-response characteristics indicated an approximate half-maximal response concentration of 230 μM for GABA (Figure 1J). In contrast, type-2 cells did not respond to the other neurotransmitters: NMDA (0%, n = 14), AMPA (0%, n = 10), and glycine (0%, n = 11) (Figures 1K, 1L, and 1M, respectively), suggesting that an analysis of the physiological role of GABAergic inputs to type-2 cells would lead to a better understanding of the mechanisms regulating activity-dependent adult neurogenesis.

In order to clarify the nature of the type-2 cells, we also characterized them immunohistochemically after the recording session. As shown in Figure 2A, all type-2 cells, as determined by their high IR values and GFP expression, were stained positively with anti-PSA-NCAM antibody. This staining pattern was never observed with type-1 cells, providing another means of identifying type-2 cells.

To determine what proportion of type-2 cells are undergoing proliferation in vivo, we next identified type-2 cells by their expression of both nestin-driven GFP and PSA-NCAM and then determined their staining pattern for anti-Ki67 antibody (Figure 2B), the expression of which is observed from the late G1 phase of the cell cycle toward the M phase (Scholzen and Gerdes, 2000). Most cells stained with the anti-Ki-67 antibody (76.40% ± 1.30% per total type-2 cells) (Figures 2C–2E). Immunohistochemically, type-1 cells displayed nestin-driven GFP expression but were PSA-NCAM negative, characteristics which are considered to define the type-1-cell population (Fukuda et al., 2003; Kempermann et al., 2004); they could also be characterized based on being GFAP positive or GLAST positive (data not shown). Only a small proportion of type-1 (GFP^+/$PSA\text{-}NCAM^-$) cells stained with anti-Ki67 antibody (25.12% ± 0.20%), indicating that few type-1 cells are cycling in vivo.

Based on these data, we can confirm that type-2 cells are actively dividing progenitor cells. Give that our electrophysiological studies have also revealed that these cells express functionally active $GABA_A$ receptors, our findings raise the intriguing possibility that GABAergic neural inputs exist on actively dividing type-2 cells and that these putative neural connections could be affecting the differentiation of adult progenitor cells.

GABAergic Inputs onto Type-2 Cells

Next, we investigated whether type-2 progenitor cells receive GABAergic inputs from the hippocampal circuitry. In whole-cell recordings of type-2 cells, we found several spontaneous currents (Figure 3A). If these currents result from neural inputs, their frequency should be increased by the application of 4-aminopyridine (4-AP), a K^+-channel blocker that augments transmitter release (Hennou et al., 2002). This was shown to indeed be the case; the frequency of mEPSC-like currents was substantially increased by the addition of 4-AP (100 μM; n = 12). These currents were completely abolished by tetrodotoxin (TTX; n = 3/3) (Figures 3B–3C), indicating the involvement of voltage-dependent Na^+ channels. The 4-AP-induced currents were also blocked by the addition of bicuculline (n = 4/4) (Figures 3D–3E). Thus, it is reasonable to assume that GABAergic inputs onto type-2 cells elicit their spontaneous currents. In accordance with our findings, Wang et al. (2005) have also very recently reported synaptic GABAergic currents in type-2 cells. In embryonic brain, progenitor cells are tonically activated by GABA release at an extrasynaptic site (LoTurco et al., 1995; Demarque et al., 2002). However, in adult hippocampus, type-2 cells did

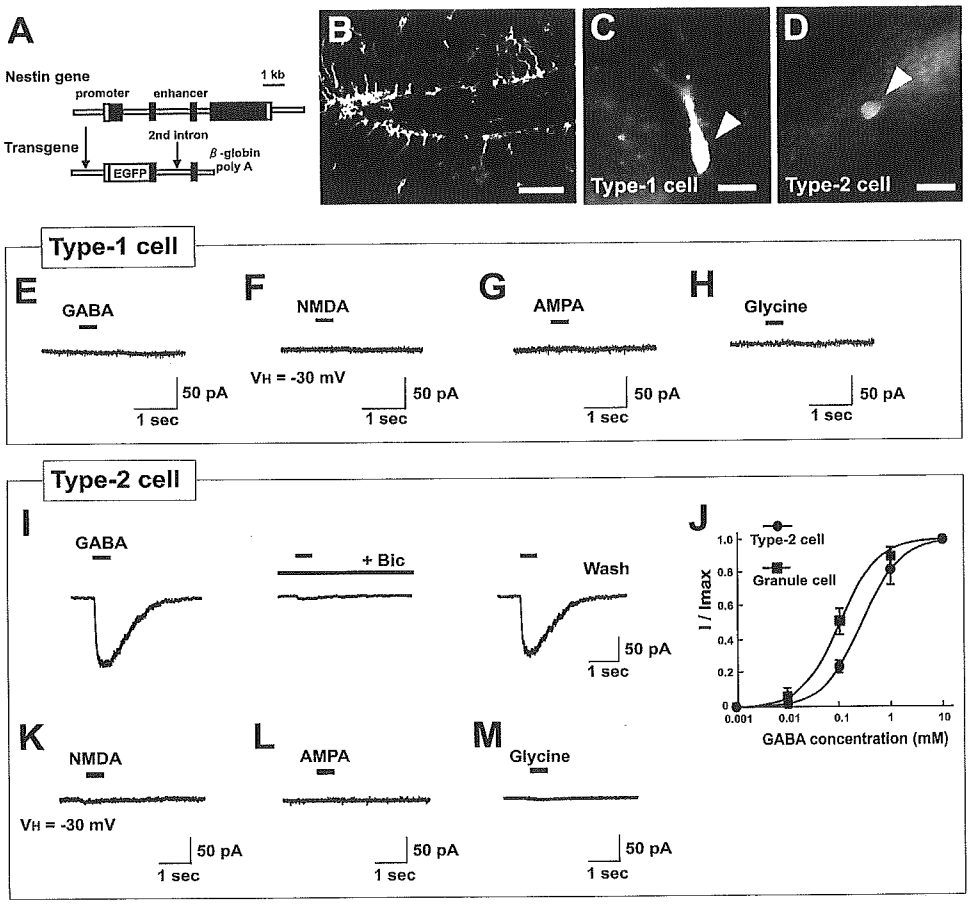

Figure 1. The Presence of Functional $GABA_A$ Receptors on Type-2 Cells

(A–D) Expression of GFP protein in both type-1 and type-2 cells in the adult dentate gyrus of nestin-GFP transgenic mice. (A) Structure of nestin-GFP transgene. (B) Confocal microscope image of the dentate gyrus of a nestin-GFP mouse. (C and D) Representative examples of fluorescence images of GFP^+ type-1 and type-2 cells, respectively.

(E–H) Lack of response of type-1 cells to stimulation by any neurotransmitter. No detectable currents were induced by GABA (1 mM [E]), NMDA (1 mM [F]), AMPA (1 mM [G]), or glycine (1 mM [H]). V_H = –60 mV (GABA, AMPA, and glycine). V_H = –30 mV (NMDA).

(I–M) Responses to different neurotransmitter-receptor agonists in type-2 cells. (I) Responses to GABA are mediated by the activation of $GABA_A$-R. GABA (200 μM) elicits an inward current. Typical recordings obtained from one cell clearly demonstrate reversible inhibition by the $GABA_A$-R antagonist, bicuculline (Bic; 50 μM). V_H = –60 mV. (J) Dose-response curve of GABA-induced currents in type-2 cells in comparison with those in mature granule neurons. In each case, the data were normalized to the maximal response and were fitted by using the Hill equation. Half-maximal concentrations and Hill coefficients were 230.6 μM and 1.12, respectively, in type-2 progenitor cells (n = 4) and 106.5 μM and 1.07 in granule cells (n = 5). No detectable currents were induced by NMDA (1 mM [K]), AMPA (1 mM [L]), or glycine (1 mM [M]). V_H = –60 mV (GABA, AMPA, and glycine). V_H = –30 mV (NMDA). All agonists were focally applied, whereas the bicuculline was bath applied. A K-gluconate-based pipette solution was used for all recordings. Scale bar, 100 μm (B) and 10 μm (C and D).

not respond to GABA in this manner because the application of bicuculline did not alter the baseline current (Figures 3F–3G).

We next tested if $GABA_A$-R currents could be generated by electrical stimulation of the local circuitry. When a single electrical stimulus was applied to the perforant pathway (main excitatory inputs into dentate gyrus), no inward currents were elicited in type-2 cells. Inward currents were, however, observed in response to a single stimulation of the hilar region (Figure 4A1), suggesting functional coupling between hilar GABAergic interneurons and type-2 cells. In control experiments, granule cells showed responses to both perforant pathway and hilar region stimulation (Figure 4A2). The reversal potential elicited by hilar stimulation was close to that estimated for Cl^- (E_{Cl} = 1.35 mV), and currents evoked by hilar stimulation were almost completely blocked by the addition of bicuculline (Figures 4B–4C).

In the dentate gyrus, interneurons are significantly activated during theta range oscillations driven by neuronal inputs from entorhinal cortex. Therefore, we asked whether GABAergic inputs on type-2 progenitor cells could be evoked by theta-burst oscillatory stimulation of the perforant pathway. Although a single stimulation of the perforant pathway did not evoke any cur-

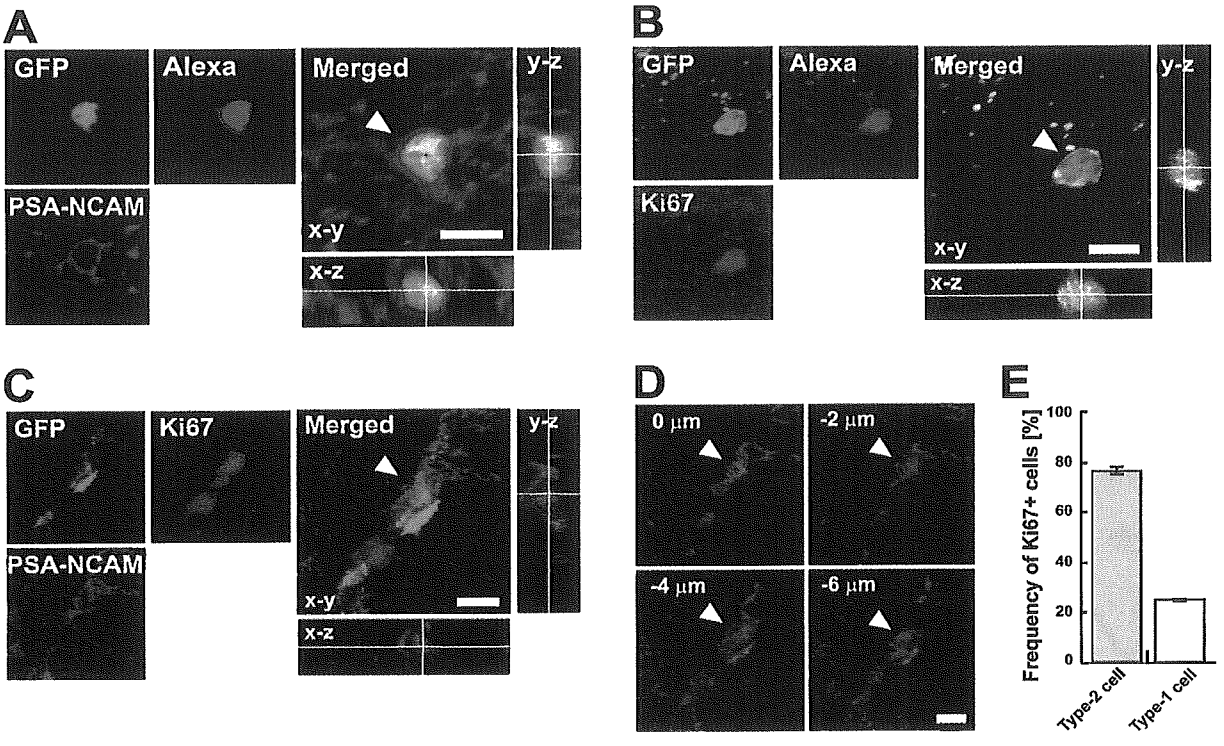

Figure 2. Immunohistochemical Evidence that Type-2 Cells Are Actively Dividing Progenitor Cells

(A) Expression of PSA-NCAM in type-2 cells after targeted recording. Type-2 cells, as determined according to electrophysiological criteria (IR > 0.5 GΩ), were PSA-NCAM positive (n = 7/7).

(B) Recorded type-2 cells (n = 3) expressed Ki67 antigen.

(C–E) Proliferating type-2 cells in the subgranular zone (SGZ). (C) Tricolor immunohistochemical analysis demonstrates the existence of type-2 cells (GFP and PSA-NCAM staining), which were actively cycling (as revealed by Ki67 antigen). (D) Z-series images from type-2 cells indicated by an arrow in Figure 2C. (E) Histogram showing that most type-2 cells ($GFP^+/PSA\text{-}NCAM^+$) were actively dividing. In contrast, only a small proportion of type-1 cells ($GFP^+/PSA\text{-}NCAM^-$) were Ki67 positive. 600 type-1 and type-2 cells from three animals (200 cells per each animal) were measured respectively. Error bars indicate standard error of the mean (SEM). Scale bar, 10 μm.

rents in type-2 cells, stimulation of the perforant pathway by a theta-burst protocol (Schmidt-Hieber et al., 2004) did elicit GABAergic currents in these cells (n = 3) (Figure 4D). This type of oscillation can also be induced experimentally by bath application of carbachol, a muscarinic acetylcholine receptor activator (Fisahn et al., 1998). As shown in Figure 4E, the bath application of carbachol triggered $GABA_A$-R-dependent mEPSC-like currents in type-2 cells. In support of this result, it has been reported that cholinergic terminals innervate the hilar region of the dentate gyrus (Dougherty and Milner, 1999). From these observations, it can be concluded that type-2 cells could receive GABAergic inputs from hippocampal interneurons, which could be activated by theta-range oscillatory hippocampal-network activity (Figure 4F).

To verify at the morphological level whether type-2 cells receive GABAergic terminals, we performed both electron and confocal microscopy studies. When viewed at the electron-microscope level, type-2 cells corresponded well to the "D cells" reported previously by Seri et al. (2001), whereas type-1 cells corresponded to "B cells" (Kempermann et al., 2004). As shown in Figures 5A and 5B, we identified nestin-GFP expressing type-2 as well as type-1 cells. We also observed some terminal-like structures close to the surface of the type-2 cells, which were identified by their GFP staining (Figure 5B′). Using confocal microscopy, we found that GABAergic terminals lay in close apposition to type-2 cells, as evaluated by the expression of the vesicular type of GABA transporter (VGAT) at the putative GABAergic terminals (Figures 5C–5G). These observations strongly suggest that type-2 cells receive some terminals from hippocampal GABAergic interneurons.

GABA Depolarizes Type-2 Cells, Inducing the Expression of NeuroD, a Positive Regulator of Neuronal Differentiation

To determine whether the opening of $GABA_A$-Rs on type-2 cells induced the membrane depolarization, we recorded from type-2 cells by using the gramicidin perforated-patch clamp technique. The application of GABA produced a membrane depolarization of approximately 10 mV in current clamp mode (Figure 6A1), and the reversal potential for Cl^- was −36.29 ± 2.56 mV (n = 13) (Figure 6B1). In control experiments, GABA application had a hyperpolarizing effect on granule cells, and their reversal potential for Cl^- was −81.56 ± 2.15 mV (n = 10).

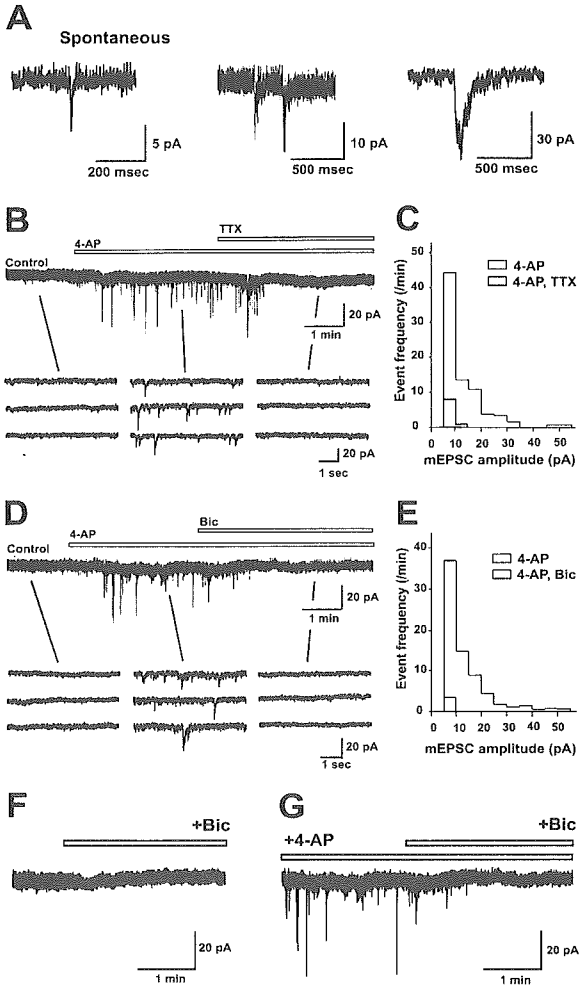

Figure 3. Spontaneous Postsynaptic-like Currents in Type-2 Cells

(A) Three examples of spontaneous synaptic-like currents recorded from type-2 cells. V_H = −60 mV. A CsCl-filled pipette solution was used.

(B and C) Bath application of 4-aminopyridine (4-AP; 100 μM) substantially increased the frequency of mEPSC-like currents in these cells. The 4-AP-induced increase in spontaneous activity was blocked by TTX (1 μM). (C) Amplitude histograms of spontaneous currents (mEPSCs) evoked by 4-AP before and during TTX application. Data were obtained from three type-2 cells (mean values).

(D and E) A $GABA_A$-R antagonist, bicuculline, blocks the generation of mEPSC-like currents in type-2 cells. Bicuculline (Bic) was bath-applied at 50 μM. (E) Amplitude histogram of 4-AP-evoked mEPSCs before and during application of bicuculline. Data were obtained from four type-2 cells (mean values).

(F and G) Absence of tonic activation of $GABA_A$-R in type-2 cells.

$[Cl^-]_i$ of type-2 cells was estimated as being 30.83 ± 2.93 mM, whereas that of granule cells was 5.38 ± 0.40 mM (Figure 6C). Furthermore, we observed the expression of Na^+-K^+-2Cl– cotransporters (NKCCs) in type-2 cells (Figure 6D), which could account for the high $[Cl^-]_i$ of immature cells. Next, we verified whether GABA application could trigger an elevation of $[Ca^{2+}]_i$ in type-2 cells. As shown in Figures 6E and 6F, GABA application resulted in an elevation of $[Ca^{2+}]_i$, a response that was blocked by the addition of Ni^{2+}, an inhibitor for voltage-gated calcium channels (Figure 6F). These results indicate that GABAergic excitation in type-2 cells leads to calcium influx via their voltage-gated calcium channels.

In order to examine whether the calcium influx triggered by $GABA_A$-R activation would be involved in the differentiation of progenitor cells, we developed a new short-term (20 hr) hippocampal slice culture protocol to evaluate the acute effect of GABAergic inputs on type-2 cells (Figure 7A) and evaluated the expression levels of a transcription factor, NeuroD (Figure 7B). NeuroD is a positive regulator of neuronal differentiation, which mediates terminal differentiation of granule cells in the dentate gyrus (Liu et al., 2000). After 20 hr of GABA stimulation, we detected a fraction of GFP^+ cells displaying elevated levels of NeuroD (fluorescence intensity > 100); this result was completely eliminated in hippocampal slices after the addition of Ni^{2+} (Figure 7C). These in vitro data strongly suggest that GABAergic excitation of type-2 cells triggers the induction of NeuroD, promoting their neuronal differentiation.

GABAergic Stimulation Promotes Neuronal Differentiation in Adult Hippocampal Progenitor Cells

To test whether GABAergic stimulation could affect the differentiation of type-2 cells in vivo, we evaluated the effects of several treatments targeted toward the GABAergic system on the proliferation and/or the differentiation of adult hippocampal progenitor cells; two agonists (phenobarbital and pentobarbital) and two antagonists (picrotoxin and pentylenetetrazole) for $GABA_A$-Rs were selected for study. To determine whether the GABAergic inputs on type-2 cells could block their cell-cycle progression, we treated mice with three injections of these drugs and subsequently labeled dividing cells by a single injection of BrdU. Treatment with a $GABA_A$-R antagonist substantially elevated the number of $BrdU^+$ type-2 cells, whereas $GABA_A$-R agonist treatment had the opposite effect. We also counted the number of $BrdU^+$ type-1 cells but did not detect any statistical difference between the five groups (data not shown). These results clearly show that GABAergic stimulation specifically affects type-2 cells and that the absence of this stimulation leads to the accumulation of dividing type-2 cells.

To evaluate whether GABAergic stimulation could promote the neuronal differentiation of adult hippocampal progenitor cells, we labeled dividing cells by a single BrdU injection and then treated mice with seven shots of $GABA_A$-R agonist or antagonist for the subsequent 7 days, based on the findings of Kempermann et al. (2004) who estimated that the length of the type-2 cell stage is about 7 days. Mice were killed 28 days after the BrdU injection, and the total number of newly born neurons in each experimental group was counted by double immunostaining with anti-BrdU and anti-calbindin, a marker for mature granule cells (Kempermann et al., 2004; Abrous et al., 2005). Data from this analysis demonstrated that the administration of $GABA_A$-R agonist significantly increased the number of new neurons in the adult dentate gyrus (Phenobarbital, 435 ± 42 $BrdU^+$ new neurons; pentobarbital, 443 ± 49; control, 296 ± 35; $p < 0.05$). This suggests that the excitation of type-2 cells by GABAergic inputs promotes their neu-

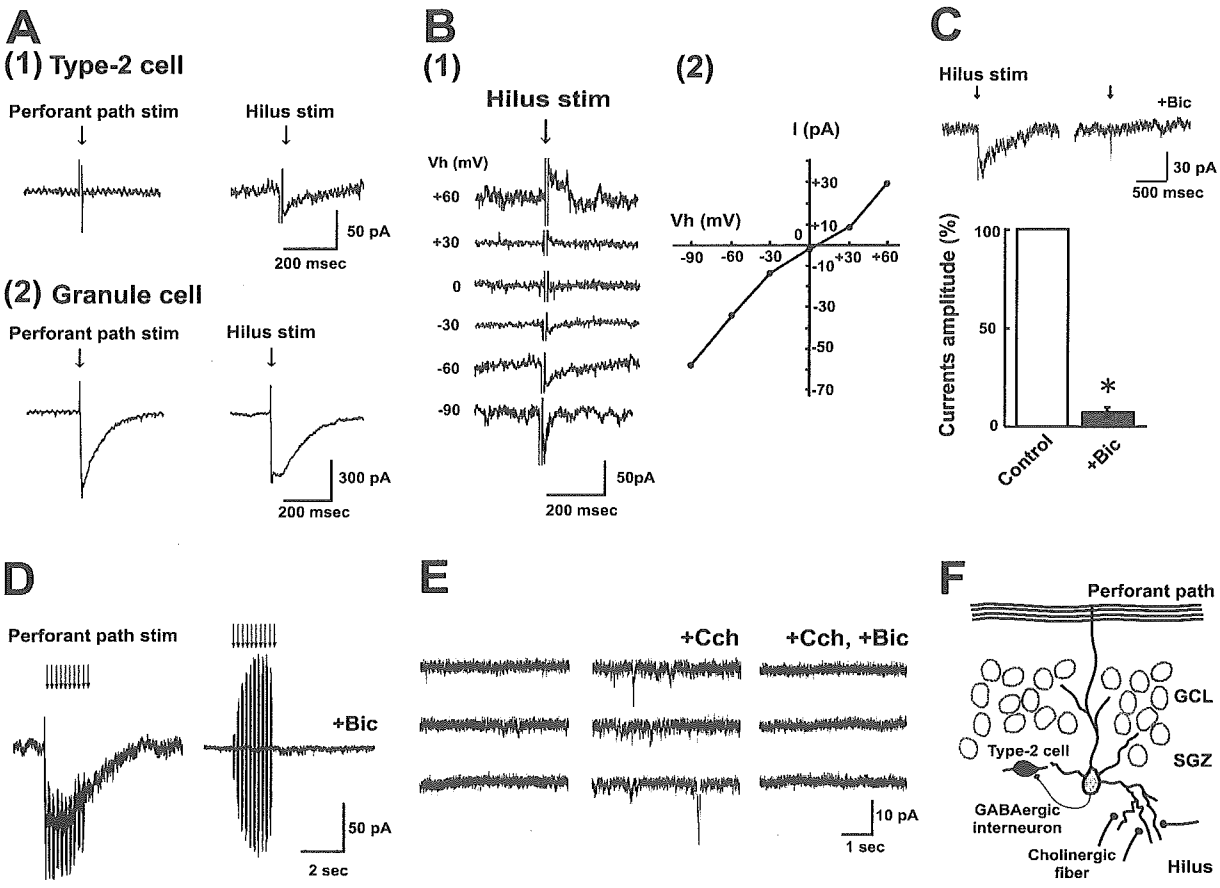

Figure 4. Stimulus-Evoked Activation of $GABA_A$-Rs on Type-2 Cells

The stimulating electrodes were located in the perforant pathway or hilar region. Cells were recorded with a CsCl pipette solution. (A1) A single perforant pathway stimulus induced no inward currents in type-2 cells, whereas a single electrical stimulus to the hilar region evoked a significant inward current. V_H = −60 mV. (A2) As a control, perforant pathway stimulation was shown to induce inward currents in mature granule cells, as did hilar stimulation. V_H = −60 mV. (B1) Stimulation-evoked currents resulting from hilar stimulation recorded at different holding potentials ranging from −90 to +60 mV. (B2) I-V relationship of the peak amplitude of stimulation-evoked currents. (C) Hilar stimulation of a type-2 cell elicited inward currents, which were blocked by bicuculline (Bic; 50 μM). V_H = −60 mV. Histogram shows a comparison of the evoked inward current amplitudes in the absence (control) and presence of bicuculline (mean ± SEM; n = 5 cells). Asterisk, $p < 0.05$. (D) $GABA_A$-R-mediated inward currents in a type-2 cell evoked by stimulation of the perforant pathway by using a theta-burst protocol. V_H = −60 mV. Similar results were obtained from two other type-2 cells. (E) Bath application of carbachol (Cch; 40 μM) increased the frequency of spontaneous synaptic current activity in type-2 cells. This activity was blocked by bicuculline (50 μM). Similar results were obtained from six other type-2 progenitor cells. (F) Schematic illustration showing a possible interaction between type-2 cells and the hippocampal GABAergic network. Activation by both perforant pathway stimulation and the cholinergic stimulation would lead to the activation of GABAergic interneurons located in the nearby dentate gyrus, causing them to release GABA toward type-2 cells. GCL, granule cell layer; SGZ, subgranular zone.

ronal differentiation and that this GABAergic stimulation consequently enhances adult hippocampal neurogenesis. In this experiment, we did not observe any significant difference in the number of total BrdU-labeled new neurons between control and $GABA_A$-R antagonist group.

Discussion

GABAergic Inputs on Adult Progenitor Cells in Dentate Gyrus

A surprising result of the present study was that in the adult dentate gyrus, even a progenitor cell receives neural inputs from the surrounding hippocampal circuitry. Interestingly, this input was GABAergic but not glutamatergic. This is perhaps not so strange given that during early hippocampal development, GABAergic synapses form prior to glutamatergic ones (Khazipov et al., 2001), whereas in the adult hippocampus, oligodendrocyte precursor cells receive GABAergic inputs (Lin and Bergles, 2004). Very recently, Overstreet Wadiche et al. (2005) have reported that newborn granule cells initially receive only GABAergic synapses. Furthermore, during adult olfactory bulb neurogenesis, new neurons also first receive GABAergic synapses and then glutamatergic ones (Carleton et al., 2003). In addition, Mayo et al. (2005) noted the expression of $GABA_A$-Rs on adult hippocampal progenitor cells at the electron microscopic level.

Although many types of axons, including the gluta-

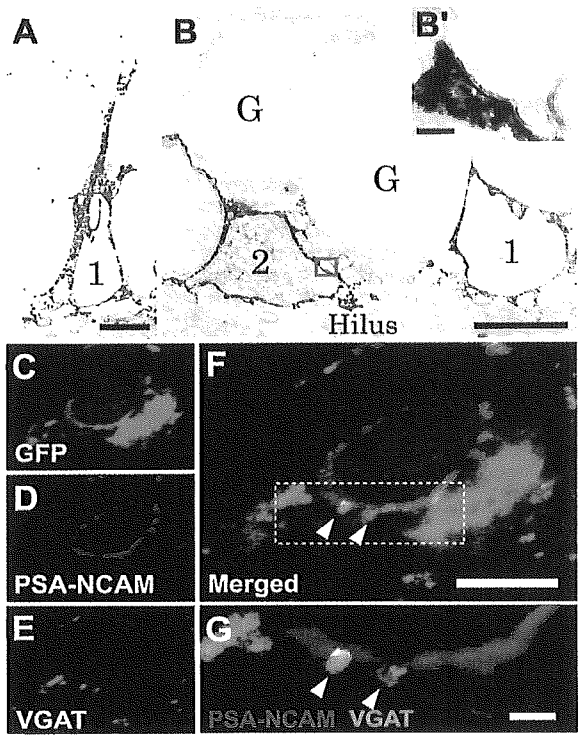

Figure 5. Morphological Evidence for GABAergic Innervation on Type-2 Cells

(A–B) Immunoelectron microscopy images of GFP$^+$ type-1 and type-2 cells. GFP was visualized with electron-dense DAB precipitation after anti-GFP staining. (A) Image showing type-1 cell with radial processes and irregular nuclei. (B) Image showing type-2 progenitor cell with dark nuclei and scant cytoplasm, as well as a type-1 cell. (B′) Enlarged view of boxed area in (B). A terminal-like structure apposed to the plasma membrane of a type-2 cell. 1, type-1 cell; 2, type-2 cell; G, granule cell. Scale bar, 4 μm (A and B); 200 nm (B′).

(C–G) Confocal images of the subgranular zone of adult mice. VGAT (vesicular GABA transporter)-expressing terminal-like structures in close contact with type-2 cells. (C) Nestin-GFP expression. (D) PSA-NCAM staining. (E) VGAT staining. (F) Merged. (G) Enlarged view of boxed area in (F), focusing on the VGAT$^+$ nerve terminals on the type-2 cell at high magnification. Note GABAergic terminals making contact on a type-2 cell. Scale bar, 5 μm (F); 1 μm (G).

matergic and cholinergic systems, penetrate into the subgranular zone of the adult dentate gyrus, only GABAergic terminals make functional contact with adult progenitor cells. This might reflect the characteristics of GABAergic neurons, which tend to connect with immature cells. Although we did not obtain any information to elucidate the nature of the putative GABAergic interneurons that send axons to type-2 cells, probable candidates may well be the basket cells or axo-axonic cells described by Freund and Buzsaki (1996). Such GABAergic interneurons receive neural inputs from perforant pathways and send their axons widely throughout the subgranular zone of the dentate gyrus (Kneisler and Dingledine, 1995). It is therefore reasonable to presume that neuronal progenitor cells located in the subgranular zone make connections with hippocampal GABAergic interneurons.

GABAergic Excitation as a Regulator of Adult Neurogenesis

In this study, we found that the excitation of adult hippocampal progenitor cells through the activation of $GABA_A$-Rs initiated calcium influx, subsequently inducing the accumulation of a neurogenic transcription factor, NeuroD. Deisseroth et al. (2004) have also reported, in an in vitro culture system, that excitatory signals exert a direct effect on dividing adult progenitor cells and have highlighted the importance of calcium signaling and NeuroD expression for neuronal differentiation. In addition, our data from BrdU pulse studies provide good evidence for the promotion of neuronal differentiation via this excitatory GABAergic system. Therefore, we can propose here a new role for the hippocampal excitatory GABAergic system in terms of its activity-dependent regulation of neuronal differentiation in the adult dentate gyrus. In support of our conclusion, Liu et al., (2005) have recently reported that GABA signaling in postnatal subventricular zone controls proliferation of adult progenitor cells.

Participation of the GABAergic system in the regulation of neurogenesis in the adult dentate gyrus has received only minimal attention to date. Given that the response of progenitor cells has been shown to be GABA-specific, GABAergic connections between these cells and GABAergic interneurons serve as the only form of neural input from the surrounding hippocampal circuitry. From the present data, it can be concluded that GABAergic interactions are the source and target of the first neural contacts formed in the hippocampal neuro-germinal zone and that GABA-mediated transmission promotes neuronal differentiation in this area.

Regulation of Adult Neurogenesis by Hippocampal Network Activity

Adult hippocampal neurogenesis is influenced by epileptic conditions (Bengzon et al., 1997; Parent et al., 1997). Patients with temporal lobe epilepsy display specific patterns of neuronal loss, with many of the missing cells being GABAergic interneurons (de Lanerolle et al., 1989; Mathern et al., 1995). Experimental models of temporal lobe epilepsy display similar patterns of interneuron loss (Obenaus et al., 1993) and reduced inhibition of dentate granule cells (Kobayashi and Buckmaster, 2003). It can therefore be postulated that in epileptic conditions, decreased release of GABA from the putative GABAergic terminal onto adult progenitor cells might positively affect the proliferation of progenitor cells in a similar manner to that observed in $GABA_A$-R antagonist-treated mice in our study.

NMDA receptor (NMDA-R) blockade in vivo also robustly increases precursor proliferation (Cameron et al., 1995; Nacher et al., 2001). This might suggest a direct influence of NMDA antagonists on adult progenitor cells; however, by means of targeted recording, neither we (this study) nor others (Wang et al., 2005) have detected any significant functional expression of NMDA-Rs on progenitor cells (type-1 and type-2 cells) in the adult dentate gyrus. It is possible that this phenomenon results from indirect effects mediated via GABAergic inputs onto transiently amplifying progenitor cells (type-2 cells). GABA release from hippocampal interneurons re-

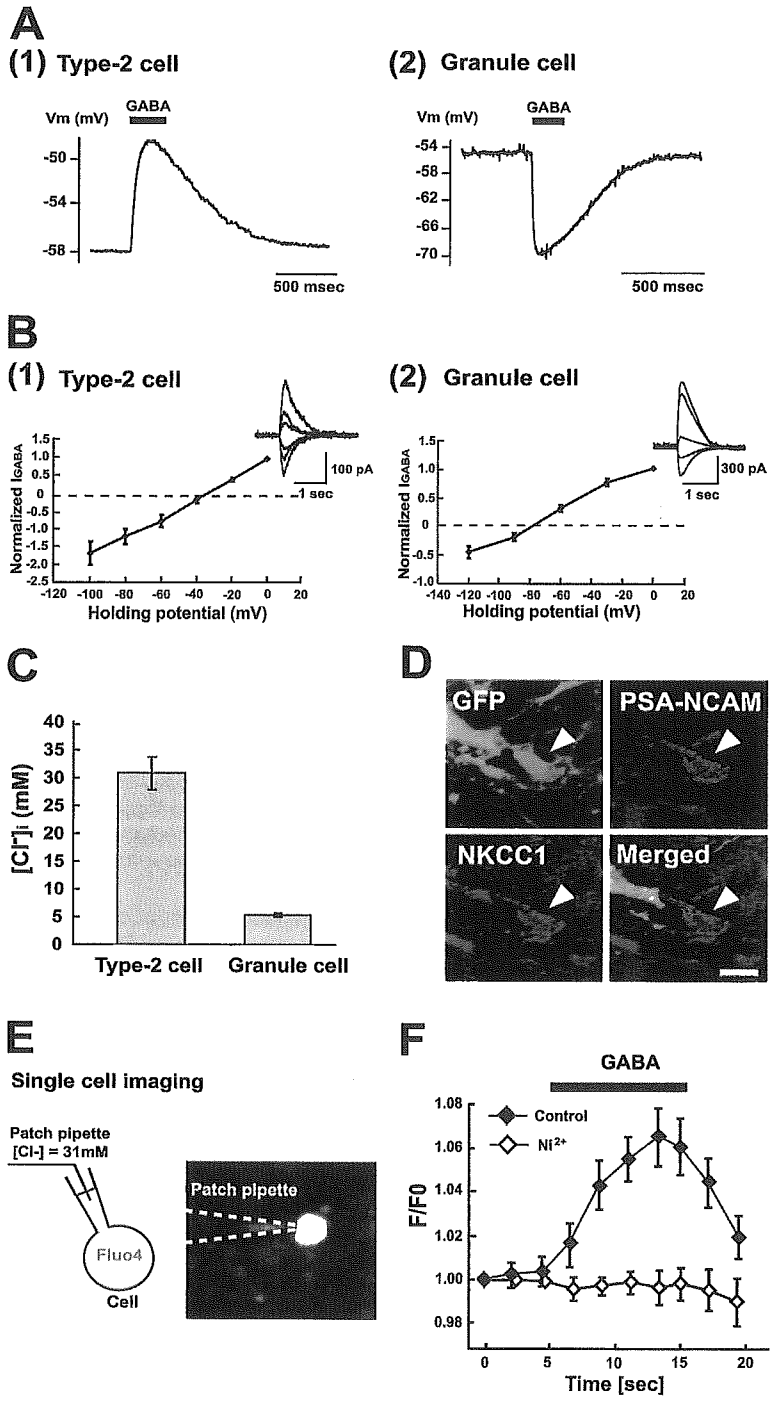

Figure 6. High $[Cl^-]_i$ Contributes to the Depolarizing Effect of GABA on Type-2 Cells

Reversal potential for chloride (E_{Cl}) was measured by the gramicidin perforated-patch technique. (A) Application of GABA produced different effects on the resting membrane potential of type-2 cells and granule cells. GABA (200 μM) induces membrane depolarization in type-2 cell (1). Recording from a granule cell shows membrane hyperpolarization after GABA application (2). (B) I-V relationships estimated from peak current amplitudes in the presence of GABA for type-2 cells (1) (n = 13) and granule cells (2) (n = 10). Currents were normalized to the peak currents recorded at V_H = 0 mV in each cell. Examples of GABA-elicited currents at different membrane potentials are shown in insert. (C) Quantitative comparison of mean estimated $[Cl^-]_i$ in type-2 cells (n = 13) and mature granule cells (n = 10). (D) Immunohistochemical detection of Na^+-K^+-$2Cl^-$ cotransporters (NKCC1) in type-2 cells. Scale bar, 10 μm. (E) Schematic diagram of single-cell Ca^{2+} imaging and fluorescence image of a Fluo-4-loaded type-2 progenitor cell; the patch pipette solution contained 31 mM Cl^- and Fluo-4. (F) GABA (200 μM) application induced an elevation of $[Ca^{2+}]_i$ in type-2 cells. The elevation of $[Ca^{2+}]_i$ was blocked by the presence of Ni^{2+} (100 μM) in the bath solution (n = 5). Error bars indicate SEM (B, C, and F).

quires NMDA-R activation (Matsuyama et al., 1997), and it has been shown that this release can be blocked by in vivo injection of the NMDA-R antagonist MK-801 (Rosenblum et al., 1999) used for the promotion of adult hippocampal neurogenesis.

GABA release from hippocampal GABAergic interneurons can be regulated by a wide variety of neurotransmitters and neuromodulators, including the serotonergic (Matsuyama et al., 1997) and cannabinoid systems (Katona et al., 1999). It has been demonstrated that the rate of adult hippocampal neurogenesis is affected by modulation of serotonergic neurotransmission (Malberg et al., 2000; Santarelli et al., 2003) and is reduced in CB1 cannabinoid-receptor knockout animals (Jin et al., 2004). Although it is still unclear how these systems regulate the rate of adult neurogenesis,

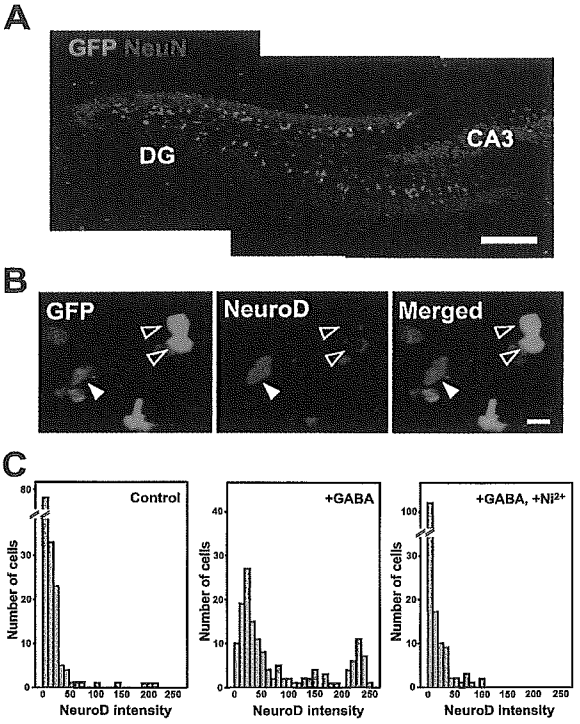

Figure 7. GABA-Mediated Ca^{2+} Influx Contributes to the Induction of NeuroD in Type-2 Cells

(A) Confocal fluorescence micrographs of a hippocampal slice cultured for 20 hr. Organotypic slices were resectioned and then immunostained. Green, GFP; red, NeuN; DG, dentate gyrus. Scale bar, 200 μm.

(B) Confocal fluorescence micrographs of NeuroD staining of GFP^+ cells after 20 hr in organotypic culture. Arrowhead shows an example of a GFP^+ cell expressing high levels of NeuroD. Open arrowheads show examples of GFP^+ cells expressing low levels of NeuroD. Scale bar, 10 μm.

(C) NeuroD intensity histogram from 150 cells in short-term hippocampal slice cultures from four animals per group: control, GABA (100 μM) treated, and both GABA and Ni^{2+} (100 μM) treated.

it is reasonable to assume that the putative interaction between GABAergic interneurons and adult progenitor cells is somehow involved.

Interestingly, the frequency of GABAergic inputs in type-2 progenitor cells is increased by application of carbachol. It has been reported that acetylcholinergic fibers from basal forebrain penetrate to this area and that these could be involved in the generation of a typical neuronal oscillation (Lee et al., 1994). Within the hippocampal formation, γ band oscillations in the theta frequency range have been implicated in exploratory behaviors and memory formation (Bragin et al., 1995; Chrobak and Buzsaki, 1998; Csicsvari et al., 2003). Particularly in the dentate gyrus, γ oscillations are related to the interneuronal network (Bragin et al., 1995). In acute brain slices, this type of oscillation can be induced experimentally by muscarinic acetylcholine receptor activation (Fisahn et al., 1998). Based on results obtained by a wide range of experimental paradigms, this neuronal oscillation has been implicated in the encoding of new memories.

In our study, we also found that stimulation of the perforant pathway by using a theta-burst protocol elicited inward currents in type-2 progenitor cells, probably because of the release of GABA from the evoked GABAergic interneurons. Taken together, our data suggest that when these oscillations appear during exploratory behaviors and memory processing, the release of GABA toward dividing type-2 progenitor cells is increased, subsequently promoting their neuronal differentiation. Indeed, it has been demonstrated that hippocampal-dependent learning tasks sometimes decrease the number of proliferating cells in the adult dentate gyrus (Dobrossy et al., 2003) in situations in which neural activity might encourage the terminal differentiation of hippocampal progenitor cells into neurons. Furthermore, environmental enrichment has been proposed to have a neurogenic effect early in neuronal development in the adult dentate gyrus (Kronenberg et al., 2003). These findings suggest that hippocampal GABAergic activity would be elevated in animals exploring enriched environments.

Conclusion

The discovery that neurogenesis occurs in the adult mammalian hippocampus has been a breakthrough in modern neuroscience, with various studies suggesting that adult hippocampal neurogenesis is involved in memory and emotion (Shors et al., 2001; Santarelli et al., 2003; Abrous et al., 2005). A number of physiological (e.g., learning) and pathological (e.g., epilepsy) conditions, which potentially modulate hippocampal GABAergic activity levels, affect the rate of adult hippocampal neurogenesis. The present study has revealed a direct interaction between dividing progenitor cells and the hippocampal GABAergic system. This provides an important insight into the neural mechanisms that underlie the modulation of neuronal differentiation, enhancing our understanding of adult hippocampal neurogenesis.

Experimental Procedures

Accute Slice Preparation

Hippocampal slices were prepared from adult (≥6 weeks old) nestin-promoter $GFP^{+/+}$ (homozygote) transgenic mice (a generous gift from Dr. Yamaguchi). Animals were deeply anesthetized with ethylether and then decapitated. The brains were removed quickly and placed in oxygenated ice-cold low-calcium artificial cerebrospinal fluid (ACSF) containing (in mM) 125 NaCl, 2.5 KCl, 0.1 $CaCl_2$, 5 $MgCl_2$, 1.25 NaH_2PO_4, 0.4 L-ascorbic acid, 25 $NaHCO_3$, and 12.5 D-glucose (95% O_2 5% CO_2 [pH 7.4]). For each experiment, coronal sections (400 μm) were obtained with a vibratome and kept for 30 min at 37°C in oxygenated standard ACSF containing (in mM) 125 NaCl, 2.5 KCl, 2 $CaCl_2$, 1.3 $MgCl_2$, 1.25 NaH_2PO_4, 0.4 L-ascorbic acid, 25 $NaHCO_3$, and 12.5 D-glucose. The slices were subsequently maintained in the same solution at room temperature until used for experiments. All experiments performed here were carried out in accordance with animal experimentation protocols approved by the Animal Care and Use Committee at the University of Tokyo.

Electrophysiological Recordings

Targeted patch-clamp recordings were performed from GFP^+ cells located in the subgranular zone of hippocampus as described previously (Fukuda et al., 2003). Type-2 cells were identified by their GFP-labeled cell body with poorly developed processes and high IR value (>0.5 GΩ).

For whole-cell recordings, patch pipettes were filled with a solu-

tion that mimicked the intracellular environment and that contained (in mM) 120 K-gluconate, 6 NaCl, 6 $CaCl_2$, 2 $MgCl_2$, 2 MgATP, 0.3 NaGTP, 10 EGTA, and 10 HEPES (pH 7.2). The intracellular solution also contained Alexa Fluor 568 hydrazide sodium salt (1/200 dilution; Molecular Probes, Eugene, OR). The IR and resting membrane potential (RMP) were measured from each cell. No compensation was made for liquid junction potentials.

For perforated patch-clamp experiments, gramicidin (Sigma, St. Louis, MO) was dissolved in dimethylsulfoxide (Sigma) and then diluted to 30 μg/ml in a KCl-based filling solution containing (in mM) 130 KCl, 5 NaCl, 0.4 $CaCl_2$, 1 $MgCl_2$, 1.1 EGTA, and 10 HEPES (pH 7.2). Procedures for recording cell electrical activity were conducted as described previously (Yoshida et al., 2004).

In experiments performed to elicit electrical activity in targeted cells, a monopolar electrode (Unique Medical, Tokyo, Japan) was inserted into the perforant pathway or hilar region. For these experiments, patch pipettes were filled with a high CsCl internal solution containing (in mM) 140 CsCl, 1 $CaCl_2$, 2 MgATP, 0.3 NaGTP, 10 EGTA, and 10 HEPES (pH 7.2). Stimulation by using a theta-burst protocol was performed as follows: four sets of brief bursts (ten stimuli at 100 Hz for 100 ms) at theta frequency (5 Hz) repeated ten times (during 2000 ms) as reported previously (Schmidt-Hieber et al., 2004).

For single-cell Ca^{2+} imaging with whole-cell recordings, the patch pipettes were filled with a Ca^{2+}-free internal solution containing (in mM) 120 K-gluconate, 19 KCl, 10 NaCl, 1 $MgCl_2$, 10 HEPES, and 5 EGTA (pH 7.2). The intracellular solution also included 50 μM Fluo-4 (Molecular Probes). For this Ca^{2+} imaging, the AquaCosmos system (Hamamatsu Photonics, Hamamatsu, Japan) was used as described previously (Okada et al., 2003; Imura et al., 2005).

GABA (Sigma), N-methyl-D-asparatic acid (NMDA; Sigma), α-amino-3-hydroxy-5-methyl-isoxazole-4-propionic acid (AMPA; Sigma), glycine (Sigma), bicuculline methiodide (Sigma), 4-aminopyridine (4-AP; Sigma), carbamylcholine chloride (carbachol; Wako, Osaka, Japan), and tetrodotoxin (TTX; Wako) were applied either by focal or bath application. In dose-response experiments, drugs were applied to the cell under investigation with a "Y-tube system" as described previously (Yoshida et al., 2004).

After the recording session, the patch electrode was carefully removed from the cell, and the slice was fixed overnight at 4°C in 4% paraformaldehyde (PFA) in phosphate buffered saline (PBS). Immunohistochemistry with antibodies against PSA-NCAM or Ki67 was performed on free-floating slices as described below.

Organotypic Slice Culture

We developed an acute adult hippocampal slice-culture protocol with slight modification of previously reported techniques (Haydar et al., 2000; Weissman et al., 2004; Kamada et al., 2004). In brief, live brain slices (400 μm) were prepared from adult mice (6–8 weeks old) as described above and placed onto Millicell-CM culture inserts (Millipore, Bedford, MA) in 6-well culture trays (Corning, Inc., NY) with medium containing 25% Hank's balanced salt solution, 25% normal horse serum, and 50% DMEM supplemented with 1.32% glucose. GABA (100 μM) and/or Ni^{2+} (100 μM) were added to the culture medium. Slices were incubated for 20 hr at 32°C with 95% O_2, 5% CO_2 and were then fixed overnight in 4% PFA. They were subsequently embedded in 5% agar gel and resectioned in 50 μm increments with a vibratome. The middle three sections of each slice were immunostained.

Immunohistochemical Staining

Animals were deeply anesthetized and perfused with PBS followed by 4% PFA in PBS and a series of sucrose-PBS solutions (10%–30%). Whole brains were sliced into 40 μm thick coronal sections with a freezing microtome. Immunohistochemistry on free-floating sections was performed as previously described (Koketsu et al., 2003). Primary antibodies and dilutions used were as follows: GFP (1:1000; rat-IgG; Nakarai Tesque, Inc., Japan and 1:1000; rabbit-IgG; Molecular Probes), PSA-NCAM (1:500; #12E3 mouse-IgM) (Seki and Arai, 1991, 1993), Ki67 (1:200; mouse-IgG; Novocastra, UK), NKCC1 (1:500; rabbit-IgG; Chemicon, Temecula, CA), VGAT (1:500; rabbit-IgG; Synaptic Systems, Germany), NeuroD (1:200; goat-IgG; Santa Cruz Biotechnology, Inc., CA), BrdU (1:200; rat-IgG; Harlan, Leicestershire, UK), calbindin (1:500; rabbit-IgG; Chemicon), or NeuN (1:1000; mouse-IgG; Chemicon). The secondary antibodies consisted of biotinylated horse anti-goat IgG (1:200; Vector Laboratories, Inc., CA), Alexa 488-conjugated goat anti-rabbit IgG (1:200; Molecular Probes), Alexa 488-conjugated goat anti-rat IgG (1:200; Molecular Probes), rhodamine-conjugated donkey anti-rabbit IgG (1:200; Chemicon), rhodamine-conjugated donkey anti-rat IgG (1:200; Jackson ImmunoResearch, West Grove, PA), rhodamine-conjugated goat anti-mouse IgM (1:200; Jackson ImmunoResearch), CY5-conjugated donkey anti-mouse IgG (1:200; ICN, Costa Mesa, CA), CY5-conjugated donkey anti-rabbit IgG (1:200; Chemicon), CY5-conjugated goat anti-mouse IgM (1:200;

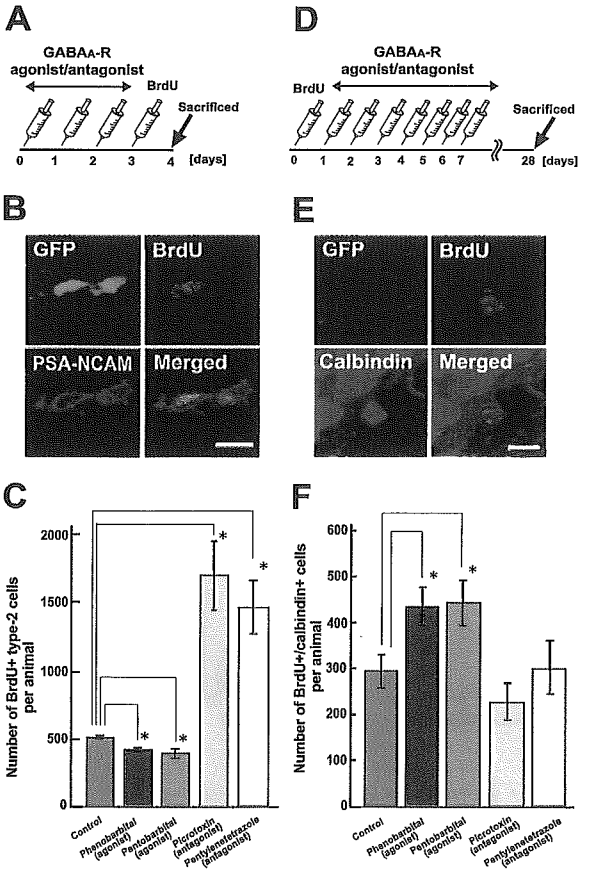

Figure 8. GABAergic Treatment Promotes the Neuronal Differentiation of Type-2 Cells

(A) Experimental paradigm assessing the proliferation of type-2 cells.

(B) Confocal micrographs of BrdU-labeled type-2 (GFP^+/PSA-$NCAM^+$) cell. Scale bar, 10 μm.

(C) The number of BrdU-labeled type-2 cells in dentate gyrus per animal. Note the significant increase of $BrdU^+$ type-2 cells in the $GABA_A$-R antagonist-treated group and the decrease of $BrdU^+$ type-2 cells in the $GABA_A$-R agonist-treated group. This increase occurred regardless of their location along the axis of the dentate gyrus.

(D) Experimental paradigm for assessing the neuronal differentiation of type-2 cells.

(E) Confocal micrographs of BrdU-labeled $calbindin^+$ cells. Scale bar, 10 μm.

(F) The number of BrdU-labeled $calbindin^+$ cells in each animal. Note the significant increase of $BrdU^+$ new neurons in the $GABA_A$-R agonist-treated groups. Error bars indicate SEM (C and F). Asterisk, $p < 0.05$, Student's t test for unpaired samples.

Jackson ImmunoResearch), and CY5-conjugated mouse anti-biotin IgG (1:200; Jackson ImmunoResearch). Images were taken with a confocal microscope (TCS SP2; Leica, Mannheim, Germany) fitted with individual filter sets for each channel. Image production was then performed with Adobe Photoshop (Adobe System, San Jose, CA).

Quantification of NeuroD Expression by Confocal Microscopic Analysis

To quantify the expression levels of NeuroD in GFP$^+$ cells, we analyzed cells immunostained with anti-NeuroD by confocal microscopy. Fields were randomly selected in which 150 GFP$^+$ cells were then analyzed. The microscope settings (e.g., laser power or pinhole size) were kept equivalent in all experiments. The average fluorescence intensities were converted into numerical settings as reported by Durand et al. (1997).

BrdU Labeling and $GABA_A$-R Agonist/Antagonist Administration

For experiments involving treatment with $GABA_A$-R agonist or antagonist, 8-week-old mice were used. To investigate the specific effect of $GABA_A$-R agonist/antagonist treatment on cell proliferation, we treated animals once daily for 3 days with an injection (i.p.) of phenobarbital (80 mg/kg in saline; n = 4), pentobarbital (50 mg/kg in saline; n = 4), pentylenetetrazole (40 mg/kg in saline; n = 4), picrotoxin (5 mg/kg in saline; n = 4), or saline (control; n = 4). 24 hr after the last treatment, animals were given 100 mg/kg BrdU (see Figure 8A); one day later, they were perfused, and the brains processed for immunohistochemistry.

Animals received a single injection of BrdU to investigate the effect of $GABA_A$-R agonist/antagonist treatment on cell differentiation. 24 hr later, they were started on a chronic regimen of phenobarbital (n = 4), pentobarbital (n = 4), pentylenetetrazole (n = 4), picrotoxin (n = 4), or saline (n = 4) once every 24 hr, totaling seven administrations (see Figure 8D). 4 weeks (28 days) after the BrdU injection, animals were perfused, and the brains processed for immunohistochemistry.

A modified unbiased stereology protocol that has previously been reported as successfully quantifying BrdU labeling (West, 1999; Malberg et al., 2000) was used. Serial sections were cut (40 μm sections) through the entire hippocampus. Every sixth section was processed for multicolor immunohistochemistry with Z-plane sectioning to confirm the colocalization of BrdU and each marker: GFP, PSA-NCAM, or calbindin. All BrdU-labeled cells located in the granule cell and subgranular layers were counted in each section by an experimenter blinded to the study code. At least eight sections per animal were examined, and the total number of BrdU-labeled cells per animal was determined and multiplied by six to obtain the total estimated number of cells per dentate gyrus. We carefully counted the number of BrdU-labeled cells within clusters and omitted cells in the outermost focal plane.

Statistical Analysis

Data were expressed as mean ± SEM. The statistical significance of the difference between means was assessed by an unpaired two-sample Student's t test, with the level of significance being set at $p < 0.05$.

Immunoelectron Microscopy

Mice were perfused with PBS followed by 4% PFA containing 0.1% glutaraldehyde in PB at room temperature. The brains were post-fixed overnight in 4% PFA in PB at 4°C. The 50-μm vibratome sections of the hippocampus prepared as described above were incubated with rabbit anti-GFP (1:500) for 48 hr at 4°C and then with peroxidase-conjugated goat polyclonal anti-rabbit IgG (1:100) for 1 hr. The sections were incubated with a 3,3′-diaminobenzidine tetrahydrochloride (DAB) solution for 15 min and then with a DAB solution containing 0.005% H_2O_2 for 10–15 min. Finally, they were post-fixed with 1% OsO_4 in PB, dehydrated, and embedded in Epok 812. Thin sections (80 nm) were mounted on uncoated grids, stained with lead citrate, and examined by electron microscopy (JEM-1230, JEOL, Tokyo, Japan; H7600, Hitachi, Tokyo, Japan).

Acknowledgments

We thank Drs. Arnold R. Kriegstein, Djoher N. Abrous, Fred H. Gage, Fiona Doetsch, James E. Goldman, Luca Santarelli, Rene Hen, Kazuyuki Aihara, Pierre-Marie Lledo, and Yehezkel Ben-Ari for informative discussions and insightful comments; Dr. Masahiro Yamaguchi for the gift of nestin-GFP transgenic mice; and Dr. Aiko Hirata for supporting EM analysis.

Received: April 14, 2004
Revised: July 5, 2005
Accepted: August 17, 2005
Published: September 14, 2005

References

Abrous, D.N., Koehl, M., and Le Moal, M. (2005). Adult neurogenesis: from precursors to network and physiology. Physiol. Rev. *85*, 523–569.

Altman, J., and Das, G.D. (1965). Autoradiographic and histological evidence of postnatal hippocampal neurogenesis in rats. J. Comp. Neurol. *124*, 319–335.

Antonopoulos, J., Pappas, I.S., and Parnavelas, J.G. (1997). Activation of GABAA receptor inhibits the proliferative effects of bFGF in cortical progenitor cells. Eur. J. Neurosci. *9*, 291–298.

Ben-Ari, Y. (2002). Excitatory actions of GABA during development: the nature of the nurture. Nat. Rev. Neurosci. *3*, 728–739.

Bengzon, J., Kokaia, Z., Elmer, E., Nanobashvili, A., Kokaia, M., and Lindvall, O. (1997). Apoptosis and proliferation of dentate gyrus neurons after single and intermittent limbic seizures. Proc. Natl. Acad. Sci. USA *94*, 10432–10437.

Blümcke, I., Schewe, J.C., Normann, S., Brustle, O., Schramm, J., Elger, C.E., and Wiestler, O.D. (2001). Increase of nestin-immunoreactive neural precursor cells in the dentate gyrus of pediatric patients with early-onset temporal lobe epilepsy. Hippocampus *11*, 311–321.

Bragin, A., Jando, G., Nadasdy, Z., Hetke, J., Wise, K., and Buzsaki, G. (1995). Gamma (40–100 Hz) oscillation in the hippocampus of the behaving rat. J. Neurosci. *15*, 47–60.

Cameron, H.A., Woolley, C.S., McEwen, B.S., and Gould, E. (1993). Differentiation of newly born neurons and glia in the dentate gyrus of the adult rat. Neuroscience *56*, 337–344.

Cameron, H.A., McEwen, B.S., and Gould, E. (1995). Regulation of adult neurogenesis by excitatory input and NMDA receptor activation in the dentate gyrus. J. Neurosci. *15*, 4687–4692.

Carleton, A., Petreanu, L.T., Lansford, R., Alvarez-Buylla, A., and Lledo, P.M. (2003). Becoming a new neuron in the adult olfactory bulb. Nat. Neurosci. *6*, 507–518.

Chrobak, J.J., and Buzsaki, G. (1998). Gamma oscillations in the entorhinal cortex of the freely behaving rat. J. Neurosci. *18*, 388–398.

Csicsvari, J., Jamieson, B., Wise, K.D., and Buzsaki, G. (2003). Mechanisms of gamma oscillations in the hippocampus of the behaving rat. Neuron *37*, 311–322.

Deisseroth, K., Singla, S., Toda, H., Monje, M., Palmer, T.D., and Malenka, R.C. (2004). Excitation-neurogenesis coupling in adult neural stem/progenitor cells. Neuron *42*, 535–552.

de Lanerolle, N.C., Kim, J.H., Robbins, R.J., and Spencer, D.D. (1989). Hippocampal interneuron loss and plasticity in human temporal lobe epilepsy. Brain Res. *495*, 387–395.

Demarque, M., Represa, A., Becq, H., Khalilov, I., Ben-Ari, Y., and Aniksztejn, L. (2002). Paracrine intercellular communication by a Ca^{2+}- and SNARE-independent release of GABA and glutamate prior to synapse formation. Neuron *36*, 1051–1061.

Dobrossy, M.D., Drapeau, E., Aurousseau, C., Le Moal, M., Piazza, P.V., and Abrous, D.N. (2003). Differential effects of learning on neurogenesis: learning increases or decreases the number of newly born cells depending on their birth date. Mol. Psychiatry *8*, 974–982.

Dougherty, K.D., and Milner, T.A. (1999). Cholinergic septal afferent terminals preferentially contact neuropeptide Y-containing interneurons compared to parvalbumin-containing interneurons in the rat dentate gyrus. J. Neurosci. *19*, 10140–10152.

Drapeau, E., Mayo, W., Aurousseau, C., Le Moal, M., Piazza, P.V., and Abrous, D.N. (2003). Spatial memory performances of aged rats in the water maze predict levels of hippocampal neurogenesis. Proc. Natl. Acad. Sci. USA *100*, 14385–14390.

Durand, B., Gao, F.B., and Raff, M. (1997). Accumulation of the cyclin-dependent kinase inhibitor p27/Kip1 and the timing of oligodendrocyte differentiation. EMBO J. *16*, 306–317.

Eriksson, P.S., Perfilieva, E., Björk-Eriksson, T., Alborn, A.M., Nordborg, C., Peterson, D.A., and Gage, F.H. (1998). Neurogenesis in the adult human hippocampus. Nat. Med. *4*, 1313–1317.

Feng, R., Rampon, C., Tang, Y.P., Shrom, D., Jin, J., Kyin, M., Sopher, B., Miller, M.W., Ware, C.B., Martin, G.M., et al. (2001). Deficient neurogenesis in forebrain-specific presenilin-1 knockout mice is associated with reduced clearance of hippocampal memory traces. Neuron *32*, 911–926.

Filippov, V., Kronenberg, G., Pivneva, T., Reuter, K., Steiner, B., Wang, L.P., Yamaguchi, M., Kettenmann, H., and Kempermann, G. (2003). Subpopulation of nestin-expressing progenitor cells in the adult murine hippocampus shows electrophysiological and morphological characteristics of astrocytes. Mol. Cell. Neurosci. *23*, 373–382.

Fisahn, A., Pike, F.G., Buhl, E.H., and Paulsen, O. (1998). Cholinergic induction of network oscillations at 40 Hz in the hippocampus in vitro. Nature *394*, 186–189.

Freund, T.F., and Buzsaki, G. (1996). Interneurons of the hippocampus. Hippocampus *6*, 347–470.

Fukuda, S., Kato, F., Tozuka, Y., Miyamoto, Y., and Hisatsune, T. (2003). Two distinct subpopulations of nestin-positive cells in adult mouse dentate gyrus. J. Neurosci. *23*, 9357–9366.

Haydar, T.F., Wang, F., Schwartz, M.L., and Rakic, P. (2000). Differentiational modulation of proliferation in the neocortical ventricular and subventricular zones. J. Neurosci. *20*, 5764–5774.

Hennou, S., Khalilov, I., Diabira, D., Ben-Ari, Y., and Gozlan, H. (2002). Early sequential formation of functional GABA(A) and glutamatergic synapses on CA1 interneurons of the rat foetal hippocampus. Eur. J. Neurosci. *16*, 197–208.

Imura, T., Kanatani, S., Fukuda, S., Miyamoto, Y., and Hisatsune, T. (2005). Layer-specific production of nitric oxide during cortical circuit formation in postnatal mouse brain. Cereb. Cortex *15*, 332–340.

Jin, K., Xie, L., Kim, S.H., Parmentier-Batteur, S., Sun, Y., Mao, X.O., Childs, J., and Greenberg, D.A. (2004). Defective adult neurogenesis in CB1 cannabinoid receptor knockout mice. Mol. Pharmacol. *66*, 204–208.

Kamada, M., Li, R.Y., Hashimoto, M., Kakuda, M., Okada, H., Koyanagi, Y., Ishizuka, T., and Yawo, H. (2004). Intrinsic and spontaneous neurogenesis in the postnatal slice culture of rat hippocampus. Eur. J. Neurosci. *20*, 2499–2508.

Katona, I., Sperlagh, B., Sik, A., Kafalvi, A., Vizi, E.S., Mackie, K., and Freund, T.F. (1999). Presynaptically located CB1 cannabinoid receptors regulate GABA release from axon terminals of specific hippocampal interneurons. J. Neurosci. *19*, 4544–4558.

Kempermann, G., Jessberger, S., Steiner, B., and Kronenberg, G. (2004). Milestones of neuronal development in the adult hippocampus. Trends Neurosci. *27*, 447–452.

Khazipov, R., Esclapez, M., Caillard, O., Bernard, C., Khalilov, I., Tyzio, R., Hirsch, J., Dzhala, V., Berger, B., and Ben-Ari, Y. (2001). Early development of neuronal activity in the primate hippocampus in utero. J. Neurosci. *21*, 9770–9781.

Kneisler, T.B., and Dingledine, R. (1995). Spontaneous and synaptic input from granule cells and the perforant path to dentate basket cells in the rat hippocampus. Hippocampus *5*, 151–164.

Kobayashi, M., and Buckmaster, P.S. (2003). Reduced inhibition of dentate granule cells in a model of temporal lobe epilepsy. J. Neurosci. *23*, 2440–2452.

Koketsu, D., Mikami, A., Miyamoto, Y., and Hisatsune, T. (2003). Nonrenewal of neurons in the cerebral neocortex of adult macaque monkeys. J. Neurosci. *23*, 937–942.

Kornack, D.R., and Rakic, P. (1999). Continuation of neurogenesis in the hippocampus of the adult macaque monkey. Proc. Natl. Acad. Sci. USA *96*, 5768–5773.

Kronenberg, G., Reuter, K., Steiner, B., Brandt, M.D., Jessberger, S., Yamaguchi, M., and Kempermann, G. (2003). Subpopulations of proliferating cells of the adult hippocampus respond differently to physiologic neurogenic stimuli. J. Comp. Neurol. *467*, 455–463.

Lee, M.G., Chrobak, J.J., Sik, A., Wiley, R.G., and Buzsaki, G. (1994). Hippocampal theta activity following selective lesion of the septal cholinergic system. Neuroscience *62*, 1033–1047.

Lin, S.C., and Bergles, D.E. (2004). Synaptic signaling between GABAergic interneurons and oligodendrocyte precursor cells in the hippocampus. Nat. Neurosci. *7*, 24–32.

Liu, M., Pleasure, S.J., Collins, A.E., Noebels, J.L., Naya, F.J., Tsai, M.J., and Lowenstein, D.H. (2000). Loss of BETA2/NeuroD leads to malformation of the dentate gyrus and epilepsy. Proc. Natl. Acad. Sci. USA *97*, 865–870.

Liu, X., Wang, Q., Haydar, T.F., and Bordey, A. (2005). Nonsynaptic GABA signaling in postnatal subventricular zone controls proliferation of GFAP-expressing progenitors. Nat. Neurosci. *8*, 1179–1187.

LoTurco, J.J., Owens, D.F., Heath, M.J., Davis, M.B., and Kriegstein, A.R. (1995). GABA and glutamate depolarize cortical progenitor cells and inhibit DNA synthesis. Neuron *15*, 1287–1298.

Malberg, J.E., Eisch, A.J., Nestler, E.J., and Duman, R.S. (2000). Chronic antidepressant treatment increases neurogenesis in adult rat hippocampus. J. Neurosci. *20*, 9104–9110.

Mathern, G.W., Babb, T.L., Pretorius, J.K., and Leite, J.P. (1995). Reactive synaptogenesis and neuron densities for neuropeptide Y, somatostatin, and glutamate decarboxylase immunoreactivity in the epileptogenic human fascia dentate. J. Neurosci. *15*, 3990–4004.

Matsuyama, S., Nei, K., and Tanaka, C. (1997). Regulation of GABA release via NMDA and 5-HT1A receptors in guinea pig dentate gyrus. Brain Res. *761*, 105–112.

Mayo, W., Lemaire, V., Malaterre, J., Rodriguez, J.J., Cayre, M., Stewart, M.G., Kharouby, M., Rougon, G., Le Moal, M., Piazza, P.V., and Abrous, D.N. (2005). Pregnenolone sulfate enhances neurogenesis and PSA-NCAM in young and aged hippocampus. Neurobiol. Aging *26*, 103–114.

Miyata, T., Kawaguchi, A., Okano, H., and Ogawa, M. (2001). Asymmetric inheritance of radial glial fibers by cortical neurons. Neuron *31*, 727–741.

Mott, D.D., Turner, D.A., Okazaki, M.M., and Lewis, D.V. (1997). Interneurons of the dentate-hilus border of the rat dentate gyrus: morphological and electrophysiological heterogeneity. J. Neurosci. *17*, 3990–4005.

Nacher, J., Rosell, D.R., Alonso-Llosa, G., and McEwen, B.S. (2001). NMDA receptor antagonist treatment induces a long-lasting increase in the number of proliferating cells, PSA-NCAM-immunoreactive granule neurons and radial glia in the adult rat dentate gyrus. Eur. J. Neurosci. *13*, 512–520.

Nguyen, L., Malgrange, B., Breuskin, I., Bettendorff, L., Moonen, G., Belachew, S., and Rigo, J.M. (2003). Autocrine/paracrine activation of the GABA(A) receptor inhibits the proliferation of neurogenic polysialylated neural cell adhesion molecule (PSA-NCAM+) precursor cells from postnatal striatum. J. Neurosci. *23*, 3278–3294.

Noctor, S.C., Flint, A.C., Weissman, T.A., Dammerman, R.S., and Kriegstein, A.R. (2001). Neurons derived from radial glial cells establish radial units in neocortex. Nature *409*, 714–720.

Noctor, S.C., Martinez-Cerdeno, V., Ivic, L., and Kriegstein, A.R. (2004). Cortical neurons arise in symmetric and asymmetric division zones and migrate through specific phases. Nat. Neurosci. *7*, 136–144.

Obenaus, A., Esclapez, M., and Houser, C.R. (1993). Loss of glutamate decarboxylase mRNA-containing neurons in the rat dentate gyrus following pilocarpine-induced seizures. J. Neurosci. *13*, 4470–4485.

Okada, H., Miyakawa, N., Mori, H., Mishina, M., Miyamoto, Y., and Hisatsune, T. (2003). NMDA receptors in cortical development are essential for the generation of coordinated increases in $[Ca^{2+}](i)$ in "neuronal domains.". Cereb. Cortex *13*, 749–757.

Overstreet Wadiche, L.S., Bromberg, D.A., Bensen, A.L., and Westbrook, G.L. (2005). GABAergic signaling to newborn neurons in dentate gyrus. J. Neurophysiol., in press. Published online July 20, 2005. 10.1152/jn.00633.2005

Owens, D.F., and Kriegstein, A.R. (2002). Is there more to GABA than synaptic inhibition? Nat. Rev. Neurosci. *3*, 715–727.

Palmer, T.D., Willhoite, A.R., and Gage, F.H. (2000). Vascular niche for adult hippocampal neurogenesis. J. Comp. Neurol. *425*, 479–494.

Parent, J.M., Yu, T.W., Leibowitz, R.T., Geschwind, D.H., Sloviter, R.S., and Lowenstein, D.H. (1997). Dentate granule cell neurogenesis is increased by seizures and contributes to aberrant network reorganization in the adult rat hippocampus. J. Neurosci. *17*, 3727–3738.

Rosenblum, K., Maroun, M., and Richter-Levin, G. (1999). Frequency-dependent inhibition in the dentate gyrus in attenuated by the NMDA receptor blocker MK-801 at doses that do not yet affect long-term potentiation. Hippocampus *9*, 491–494.

Santarelli, L., Saxe, M., Gross, C., Surget, A., Battaglia, F., Dulawa, S., Weisstaub, N., Lee, J., Duman, R., Arancio, O., et al. (2003). Requirement of hippocampal neurogenesis for the behavioral effects of antidepressants. Science *301*, 805–809.

Schmidt-Hieber, C., Jonas, P., and Bischofberger, J. (2004). Enhanced synaptic plasticity in newly generated granule cells of the adult hippocampus. Nature *429*, 184–187.

Scholzen, T., and Gerdes, J. (2000). The Ki-67 proteins: from the known and unknown. J. Cell. Physiol. *182*, 311–322.

Seki, T. (2002a). Expression patterns of immature neuronal markers PSA-NCAM, CRMP-4 and NeuroD in the hippocampus of young adult and aged rodents. J. Neurosci. Res. *70*, 327–334.

Seki, T. (2002b). Hippocampal adult neurogenesis occurs in a microenvironment provided by PSA-NCAM-expressing immature neurons. J. Neurosci. Res. *69*, 772–783.

Seki, T., and Arai, Y. (1991). The persistent expression of a highly polysialylated NCAM in the dentate gyrus of the adult rat. Neurosci. Res. *12*, 503–513.

Seki, T., and Arai, Y. (1993). Highly polysialylated neural cell adhesion molecule (NCAM-H) is expressed by newly generated granule cells in the dentate gyrus of the adult rat. J. Neurosci. *13*, 2351–2358.

Seri, B., Garcia-Verdugo, J.M., McEwen, B.S., and Alvarez-Buylla, A. (2001). Astrocyte give rise to new neurons in the adult mammalian hippocampus. J. Neurosci. *21*, 7153–7160.

Seri, B., Garcia-Verdugo, J.M., Collado-Morente, L., McEwen, B.S., and Alvarez-Buylla, A. (2004). Cell types, lineage, and architecture of the germinal zone in the adult dentate gyrus. J. Comp. Neurol. *25*, 359–378.

Shors, T.J., Mlesegaes, G., Beylin, A., Zhao, M., Rydel, T., and Gould, E. (2001). Neurogenesis in the adult is involved in the formation of trace memories. Nature *410*, 372–376.

Steiner, B., Kronenberg, G., Jessberger, S., Brandt, M.D., Reuter, K., and Kempermann, G. (2004). Differential regulation of gliogenesis in the context of adult hippocampal neurogenesis in mice. Glia *46*, 41–52.

van Praag, H., Schinder, A.F., Christie, B.R., Toni, N., Palmer, T.D., and Gage, F.H. (2002). Functional neurogenesis in the adult hippocampus. Nature *415*, 1030–1034.

Wang, L.-P., Kempermann, G., and Kettenmann, H. (2005). A subpopulation of precursor cells in the mouse dentate gyrus receives synaptic GABAergic input. Mol. Cell. Neurosci. *29*, 181–189.

Weissman, T.A., Riquelme, P.A., Ivic, L., Flint, A.C., and Kriegstein, A.R. (2004). Calcium waves propagate through radial glial cells and modulate proliferation in the developing neocortex. Neuron *43*, 647–661.

West, M.J. (1999). Stereological methods for estimating the total number of neurons and synapses: issues of precision and bias. Trends Neurosci. *22*, 51–61.

Yamaguchi, M., Saito, H., Suzuki, M., and Mori, K. (2000). Visualization of neurogenesis in the central nervous system using nestin promoter-GFP transgenic mice. Neuroreport *11*, 1991–1996.

Yoshida, M., Fukuda, S., Tozuka, Y., Miyamoto, Y., and Hisatsune, T. (2004). Developmental shift in bi-directional functions of taurine-sensitive chloride channels during circuit formation in postnatal mouse brain. J. Neurobiol. *60*, 166–175.

Zimmerman, L., Parr, B., Lendahl, U., Cunningham, M., McKay, R., Gavin, B., Mann, J., Vassileva, G., and McMahon, A. (1994). Independent regulatory elements in the nestin gene direct transgene expression to neural stem cells or muscle precursors. Neuron *12*, 11–24.

Cerebral Cortex March 2005;15:332-340
doi:10.1093/cercor/bhh135
Advance Access publication July 21, 2004

Layer-specific Production of Nitric Oxide during Cortical Circuit Formation in Postnatal Mouse Brain

Taiko Imura, Shigeaki Kanatani, Satoshi Fukuda, Yusei Miyamoto and Tatsuhiro Hisatsune

Department of Integrated Biosciences, University of Tokyo, Kashiwa 277-8562, Japan

In the developing cerebral cortex, neuronal nitric oxide synthase (nNOS) is expressed abundantly, but temporarily. During the early postnatal stage, cortical neurons located in the multi-layered structure of the cortical plate start forming well-organized cortical circuits, but little is known about the molecular machinery for layer-specific circuit formation. To address the involvement of nitric oxide (NO), we utilized a new NO indicator (DAR-4M) and developed a protocol for the real-time imaging of NO produced in fresh cortical slices upon *N*-methyl-D-aspartic acid stimulation. At postnatal day 0 (P0), NO production was restricted to the deep layers (layers V and VI) of the somatosensory cortex where transient synapses are formed. At P10, the production of NO was expanded to layer IV where large numbers of thalamocortical axons form synapses. The pattern of NO production could correspond to active sites for synaptic formation. This study is the first clear demonstration of NO production in the postnatal mouse neocortex. The findings presented may reflect a function of NO in relation to the layer-specific development of neural circuits in the neocortex.

Keywords: Ca imaging, neuronal nitric oxide synthase, nitric oxide imaging, NMDA stimulation, somatosensory cortex

Introduction

Rodent thalamocortical networks are formed according to genetically oriented and/or activity-dependent processes that take place during postnatal development (Sur and Leamey, 2001; Lopez-Bendito and Molnar, 2003). Thalamocortical axons penetrate through the internal capsule in the prenatal stage, eventually connecting with layer IV cortical neurons (Higashi *et al.*, 1999; Molnar *et al.*, 2000). Molecular mechanisms that govern the projection of thalamocortical axons to the developing subplate have been studied extensively (Lopez-Bendito and Molnar, 2003); however, the 'machinery' by which connections between thalamocortical axons and cortical neurons are made is mostly unknown. In thalamocortical connections of the somatosensory system, peripheral activities stimulate the sprouting of thalamocortical axons. The *N*-methyl-D-aspartic acid (NMDA)-receptor is a candidate for mediating such an activity-dependent development of neural circuitry. Iwasato *et al.* have developed a cortex-specific deletion of the *NMDA-R1* gene, and have demonstrated the disruption of barrel boundaries in the somatosensory cortex of *NMDA-R1* knock-out mice (Iwasato *et al.*, 2000). In a subsequent study, defective sprouting of thalamocortical axons in this strain was demonstrated (Datwani *et al.*, 2002).

Nitric oxide (NO) is a gaseous neurotransmitter produced by neuronal nitric oxide synthase (nNOS). In the developing cortex, nNOS is abundantly, but temporarily, expressed in the developing cortical plate (Bredt and Snyder, 1994; Santacana *et al.*, 1998). NOS activity at this stage has been suggested by NADPH-diaphorase (NADPH-d) histochemistry in both experimental animals and human fetus (Bredt *et al.*, 1991; Dawson *et al.*, 1991; Derer and Derer., 1993; Mitrovic and Schachner, 1996; Van Eden *et al.*, 1996; Yan *et al.*, 1996; Vercelli at al., 1999). It is well accepted that nNOS requires elevation of the calcium concentration in order to be activated (Knowles *et al.*, 1989; Bredt and Snyder, 1990). The elevation of intracellular calcium concentration ($[Ca^{2+}]_i$) after the opening of NMDA-receptor channels is regarded as a typical upstream signal leading to NO production (Garthwaite *et al.*, 1988; Bredts and Snyder, 1989; Bohme *et al.*, 1991). During development, NO is thought to act as a retrograde signal, serving to stabilize and refine afferent connections via an activity-dependent mechanism (Wu *et al.*, 1994; Cramer *et al.*, 1996). In both young and adult primates, region- and layer-specific NOS activity in cerebral cortex has been suggested from anti-nNOS staining and NADPH-d histochemistry studies (Rivier and Clarke, 1997; Wong-Riley *et al.*, 1998; Barone and Kennedy, 2000; Wiencken and Casagrande, 2000; Benavides-Piccione and DeFelipe, 2003). As mentioned above, circuit-specific production of NO has been suggested both in developmental and adult cerebral cortex; however, the production of NO from such a cortical tissue had not been demonstrated yet.

Since NO is a gaseous molecule with a very short half-life, the dynamics of NO in developing cerebral cortex have been difficult to measure in a real-time format. DAR-4M is a newly developed NO indicator with a structure based on the rhodamine chromophore, whose signal-to-noise ratio and the pH sensitivity properties have been improved (Kojima *et al.*, 2001) with respect to conventional NO indicators (Kojima *et al.*, 1998a,b). In this communication, we show for the first time the real-time spectrum of NO production in the developing cortical plate, with fine spatiotemporal resolution allowing identification of the layer-specific release of NO.

Materials and Methods

Preparation of Slices

ICR mice [postnatal day (P) 0, P10 and P30; Sankyo Laboratory Service, Tokyo, Japan] were anesthetized by hypothermia or with ether, and whole brains were dissected free and placed in cold low-calcium artificial cerebrospinal fluid (ACSF). All experiments were carried out in accordance with the guidelines for Animal Experiments of the Graduate School of Frontier Sciences, The University of Tokyo. Coronal slices (400 μm) that included the developing somatosensory cortex (Bayer and Altman, 1991; Schambra *et al.*, 1992; Jacobowitz and Abbott, 1998) and tangential slices (400 μm) that included the barrel in layer IV of somatosensory cortex of P10 mice (Welker and Woolsey, 1974) were prepared in low-calcium ACSF at 0°C with the aid of a microslicer (DOSAKA EM, Kyoto, Japan). The slices were then incubated in standard

ACSF at 37°C for 30 min. The low-calcium ACSF contained 124 mM NaCl, 2.5 mM KCl, 26 mM $NaHCO_3$, 4.5 mM $MgCl_2$, 1.25 mM NaH_2PO_4, 0.1 mM $CaCl_2$ and 10 mM glucose. Standard ACSF used in experiments contained 124 mM NaCl, 2.5 mM KCl, 26 mM $NaHCO_3$, 1 mM $MgCl_2$, 1.25 mM NaH_2PO_4, 2 mM $CaCl_2$ and 10 mM glucose. Each type of ACSF was equilibrated with 95% O_2/5% CO_2.

Loading of Fluorescence Indicator

In order to investigate the location of NO production, real-time NO imaging was performed using a fluorescent NO-indicator. A selective fluorescent indicator for NO (DAF-2; Kojima *et al.*, 1998a) was developed to visualize the location of NO production (Kojima *et al.*, 1998b), in which DAF-2 traps NO and turns to DAF-2 T (triazole form of DAF-2) emitting a strong fluorescence signal. Initially, we had used DAF-2 in the real-time imaging of NO in the somatosensory cortex of developing mouse, but a satisfactory result could not be obtained, probably due to the insufficient production of NO in this preparation and the low signal-to-noise ratio of the DAF-2 indicator. A further major problem was associated with the fact that the laser light produces a strong fluorescence signal, presumably from photoactivated production of DAF-2 T. Indeed, it was previously reported that DAF-2 is sensitive to photoactivation (Broillet *et al.*, 2001).

For these reasons, we used a newly developed alternative NO-indicator, DAR-4M (Kojima *et al.*, 2001), for NO imaging of developing brain slices. After 30 min incubation, the slices were loaded for 90 min at 37°C with DAR-4M AM (10 μM) in standard ACSF containing 0.01% cremophor EL. Loaded slices were rinsed in standard ACSF for 30 min at 37°C prior to use in imaging experiments. DAR-4M reacts irreversibly with NO to produce the triazole form of DAR-4M, namely DAR-4M T. We did not observe any photoactivated production of strong fluorescence signal. For dual imaging of NO and $[Ca^{2+}]_i$, slices were incubated simultaneously with DAR-4M AM (10 μM) and fluo-4 AM (10 μM) in 0.01% cremophor EL for 90 min at 37°C. Calcium imaging for cortical slices was based on the method reported previously (Okada *et al.*, 2003).

Imaging of Slices by Confocal Laser Scanning Microscopy

Each slice used for imaging experiments was placed in a purpose-built perfusion chamber (depth: 4 mm; diameter: 14 mm: volume: 300 μl, flow rate: 55.56 μl/s) and held in position with a slice anchor. The slices were examined using a confocal laser scanning microscope (TCS-SL, Leica, Mannheim, Germany) equipped with adjustable slits enabling the user to specify the wavelength range for the detection of emitted light. In NO imaging, loaded slices were excited with 543 nm light and the emitted signal was collected in the range of 575–700 nm, for the maximum collection from the DAR-4M T-derived fluorescence signal. In NO and Ca^{2+} dual imaging, the collection spectrum for DAR-4M T was changed from 575–700 nm to 600–700 nm, because of the weak signal from Ca^{2+}, which is excited at 543 nm and collected at 575–600nm. For the collection from Ca^{2+}-related fluorescence signals, slices were excited at 488 nm and signals were collected at 500–550 nm. In this condition, we did not detect any signal from DAR-4M T. In NO and Ca^{2+} dual imaging, each scan was performed separately as a Sequential mode (TCS SL system, Leica).

In each imaging protocol, optical signals were collected with a TCS SL system (Leica) and fluorescence images were obtained sequentially at intervals of 6 s. A frame was created from the average of two scans (it took 1.663 s to perform one scan). To evaluate whether or not the NO-indicator DAR-4M was evenly distributed throughout fresh cortical slices, we used a synthetic NO donor, NOC12, and confirmed that the DAR-4M-related fluorescence signals were detected in all cortical layers and areas just after NOC12 application (data not shown). To visualize the activity-dependent production of NO, NMDA (Sigma, St Louis, MO) (100 μM) was bath-applied.

In NO imaging with treatment of inhibitors, DAR-4M-loaded cortical slices were treated with N^G-nitro-L-arginine methyl ester (L-NAME; Dojindo, Kumamoto, Japan) (5 mM), NOS universal inhibitor, or 7-nitroindazole (7-NI; Sigma, St Louis, MO) (100 μM), nNOS-specific inhibitor, before starting NO imaging for 30 min. After the treatment, the slices were placed in chamber and perfused with ACSF including inhibitors during NO imaging respectively. NMDA (100 μM) was dissolved in ACSF including inhibitors, and bath-applied. In NO imaging under the condition without inhibitors, all drugs were dissolved in ACSF.

Data Analysis

Two regions (region1, region2) of the fluorescence images were selected as upper layers and deep layers of the cortical plate by means of the easily identifiable granule cell zone. Each region was subdivided into five subdivisions (a–e). The fluorescence intensity of each subdivision was converted into values using the Quantification function of the TCS SL system (Leica), following which the values of fluorescence intensity for each region were calculated using Microsoft Excel software as the average of those five subdivisions. Since DAR-4M reacts irreversibly with NO to form DAR-4M T, the level of DAR-4M T production per unit time was obtained by subtracting from the fluorescence intensity at one point from that of the point which preceded it. Time-points were graphed for every five calculated values. Levels of calcium response and NO production were estimated by subtracting the fluorescence intensity at the baseline from that at the peak of the calcium response and at the end of NO imaging respectively. The calculated values of calcium response and NO production were compared between upper and deep layers.

Single Cell Imaging

Coronal slices of P10 mice were prepared as described above. One slice was fixed in a recording chamber (~0.2 ml volume, RC-26GLP; Warner Instruments, Hamden, CT) under nylon strings attached to a U-shaped platinum frame, then submerged in, and continuously perfused with, the standard ACSF at a flow rate of 1–2 ml/min. Neuronal cells in layer IV could be identified as cells situated between large pyramidal neurons at layer V and small pyramidal neurons at layer II/III.

Patch electrodes were fabricated from borosilicate glass capillaries of 1.2 mm outer diameter (1B120F-4; World Precision Instruments, Sarasota, FL) with a programmable puller (P-87; Sutter Instrument, Novato, CA). The composition of the pipette internal solution was (mM): potassium gluconate, 120; NaCl, 6; $CaCl_2$, 5; $MgCl_2$, 2; MgATP, 2; NaGTP, 0.3; EGTA, 10; HEPES, 10; pH 7.2 with KOH. The intracellular solution also included 10 mM DAR-4M for NO imaging of the cells recorded. The tip resistance of the electrodes ranged from 5 to 10 MΩ when filled with this solution. Data were recorded at room temperature with a CEZ-2400 amplifier (Nihon-kohden, Tokyo, Japan). The membrane current was sampled on-line at 4 kHz (PowerLab; AD Instruments, Grand Junction, CO) after filtering at 2 kHz to achieve synchrony with NO imaging using AQUACOSMOS system (Hamamatsu) (Okada *et al.*, 2003) and stored on the hard disk of a personal computer. The data were analyzed off-line with Igor Pro 4.01 (WaveMetrics, Lake Oswego, OR). NMDA was pressure-applied locally using a PicoPump (PV820; World Precison Instruments) via a glass pipette positioned ~30 μm from the soma of the recorded cell (Fukuda *et al.*, 2003).

Immunohistochemistry

Mice [postnatal day (P) 0] were perfused with phosphate-buffered saline (PBS) (in mM: 137 NaCl, 8.1 NaH_2PO_4, 2.68 KCl, 1.47 KH_2PO_4) followed by 4% freshly depolymerized paraformaldehyde in PBS. Brains were removed and postfixed in 4% paraformaldehyde in PBS for 1 h–1 day at 4°C. Tissues were cryoprotected for 1–2 days and then embedded with OCT compound. Coronal sections (40 μm) were then cut on a cryostat (HM505E; MICROM, Walldorf, Germany). For the immunostaining for nNOS protein, the sections were washed in PBS for 10 min and then blocked for 30 min in blocking buffer containing 5% normal goat serum and 0.3% Triton X-100 in PBS. The sections were incubated for 1 day at 4°C with anti-mouse nNOS polyclonal antibody (rabbit IgG, 1:1000 dilution) and then washed with PBS three times and incubated for 2 h at room temperature with Alexa488-conjugated goat anti-rabbit IgG antibody (1:5000 dilution; Molecular Probes, Eugene, OR). Primary antibodies and secondary antibodies were diluted in buffer containing 5% normal goat serum and 0.1% Triton X-100 in PBS. After being washed three times, the sections were mounted with Immu-mount. Fluorescence images were obtained with a TCS SP2 system (Leica).

After NO imaging, the coronal brain slices were used for NADPH-d histochemistry, Toluidine Blue staining and immunohistochemistry for nNOS protein. The slices were postfixed in 4% paraformaldehyde in PBS for 30 min, and then were rinsed in ice-cold PBS for 10 min. The slices were cryoprotected for 1–2 days and then embedded with OCT compound. The embedded slices were resectioned at a thickness of

16 μm on cryostat and resectioned slices were mounted on poly-L-lysine-coated slides. For NADPH-d histochemistry, the resectioned slice was incubated at 37°C for 2-3 h in a solution containing 5 mg nitroblue tetrazolium (NBT; Wako; Osaka, Japan) and 20 mg β-nicotinamide adenine dinucleotide phosphate (NADPH; Oriental Yeast, Tokyo, Japan) in 20 ml of PBS. The slice was then rinsed in PBS, dehydrated, cleared in xylene and coverslipped in Entellan mounting media. Toluidine Blue Nissl staining, when performed, was carried out by following standard protocols (Sugitani *et al.*, 2002). Immunohistochemical staining for nNOS protein was performed as described above.

After the NO imaging of the tangential slices of P10 mouse, the slices were used for cytochrome oxidase (CO) histochemistry. The slices were postfixed in 4% paraformaldehyde in PB for 30-60 min, and were then cryoprotected for 1-2 days. The slices were incubated at 37°C for 1-3 h in a solution containing 10 mg 3,3′-diaminobenzidine tetrahydrochloride (DAB; Sigma), 0.8 g sucrose and 6 mg cytochrome C (Wako) in 20 ml of PB. After the incubation, the slices were rinsed in PBS. Images of sections stained for TB, NADPH-d and CO histochemistry were acquired using microscope (BX-50WI, Olympus, Tokyo, Japan), fitting with a CAMEDIA digital camera (Olympus).

Results

Production of NO in Developing Cerebral Cortex

Previous studies have clearly demonstrated that nNOS is expressed temporarily and abundantly in the cerebral neocortex during development (Bredt and Snyder, 1994; Santacana *et al.*, 1998; Terada *et al.*, 2001), but there is some discrepancy between these studies concerning the spatiotemporal expression of nNOS. In the light of this, we first assessed the expression of nNOS in the developing cerebral cortex by using early postnatal stage (P0) mice. Animals from this developmental stage were chosen because all three of the above studies presented nNOS immunostaining of brain slices from P0 animals. As shown in Figure 1, two types of nNOS staining are present in the cortical plate. One type corresponds to a particular cortical plate neuron expressing nNOS proteins extensively, while in the other, weak levels of staining reflect the perinuclear localization of nNOS in cortical plate neurons as reported by Bredt and Snyder (1994). Similar patterns of NADPH-d staining have been reported in developing rat cortex (Vercelli *et al.*, 1999).

To assess which type of nNOS actually produces NO, real-time NO imaging with high spatiotemporal resolution was used to detect NO in the developing cerebral cortex by means of the NO fluorescence indicator, DAR-4M. A DAR-4M-loaded fresh brain slice that contained the somatosensory cortex was stimulated by the application of NMDA. Very little DAR-4M fluorescence signal could be detected prior to NMDA application (Fig. 2*A*), but a significant increase in the fluorescence signal within relatively deep cortical layers was detected after NMDA administration (Fig. 2*B*). In order to analyze the location of NO production, we selected two regions in the cortical plate (region1: upper layers as supragranular layer; region2: deep layers as infragranular layer) and compared the fluorescence intensity of the NO indicator in each region (Fig. 2*C,D*). NMDA-induced NO production was relatively higher in the deep layers compared to the upper layers (Fig. 2*C*). Using the NO-imaging technique, we did not detect NO production from any single, strongly stained nNOS-positive neurons, suggesting that such neurons do not produce NO under these conditions. The amount of NO production per unit of time in the deep layers was more than that in the upper layers (Fig. 2*D*). This is the first visual demonstration of the production of NO in the developing cortical plate.

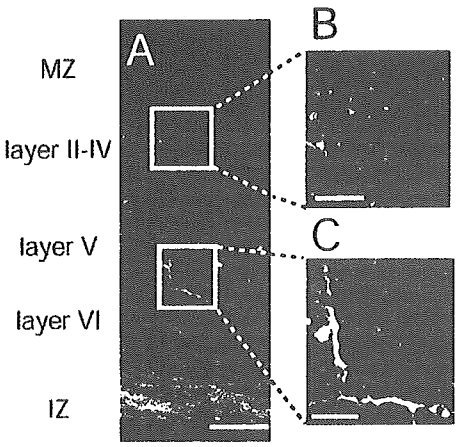

Figure 1. Immunohistochemistry of nNOS in the primary somatosensory neocortex of neonatal mice. The image was observed with a 20× objective lens (*A*) and a 63× lens (*B, C*). (*B, C*) Enlarged images from the area in (*A*) surrounded by boxes. IZ, intermediate zone; MZ, marginal zone. Scale bar: 80 μm (*A*) and 20 μm (*B, C*). Note that two neurons heavily expressing nNOS are shown in (*C*).

Recently, it has also been reported that brain endothelial cells expressed NMDA receptors (Sharp *et al.*, 2003). Since endothelial cells possessing endothelial NOS (eNOS) could be activated by NMDA, NO might be produced from eNOS. To verify whether NO was mainly produced from nNOS, we performed NO imaging with a set of inhibitors: L-NAME (a universal NOS inhibitor), and 7-NI (a nNOS-specific inhibitor) (Fig. 3). NO production in the deep layers was observed when no inhibitors were used (control condition), as shown in Figure 2. NO production in slices treated with L-NAME or 7-NI was weaker than in control slices. As shown in Figure3*B*, NO production in deep layers of slices treated with 7-NI and L-NAME decreased to 31 and 15% of that in control slices respectively. Therefore, these data suggested that the NO production stimulated by NMDA mainly originated from nNOS.

NO-Calcium Dual Imaging Demonstrates Layer-specific Production of Nitric Oxide in Developing Cortical Plate

It is known that nNOS activation requires the elevation of $[Ca^{2+}]_i$ (Garthwaite *et al.*, 1988; Bohme *et al.*, 1991) to produce NO. The reason for NO production only in the deep layers of the cortical plate could stem from a layer-specific NMDA receptor-mediated calcium influx and subsequent elevation of $[Ca^{2+}]_i$ in neurons of the developing cortical plate. To test this hypothesis, we developed a dual imaging system for the simultaneous measurement of NO and $[Ca^{2+}]$ in order to assess the correlation between calcium influx and NO production in the developing cortical plate.

During the application of NMDA, calcium influx was evoked both in the upper layers and deep layers (Fig. 4*A-C*), but the response was more robust in the upper cortical layers. However, NO was produced only in the deep cortical layers (Fig. 4*E-G*), as shown in Figure 2. The dynamics of calcium influx and NO production are shown in Figure 4*D,H*, where it can clearly be seen that the production of NO was not detected in the upper layers in spite of the rapid elevation of $[Ca^{2+}]_i$ in this region. There are several possibilities to explain this finding. (i) This might have been stemmed from the lack of a related molecule in the upper cortical layers. A candidate molecule is calcineurin,

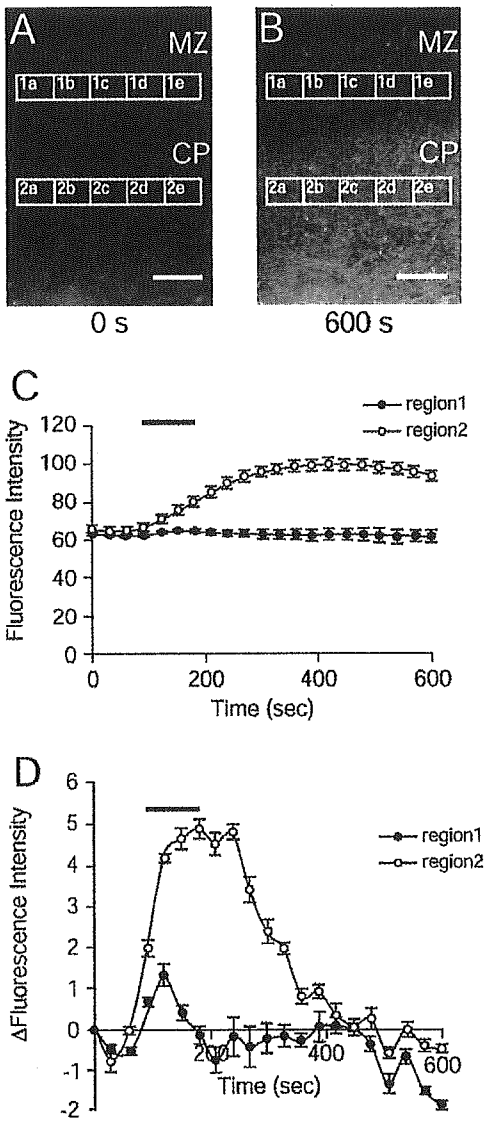

Figure 2. The production of NO stimulated by NMDA in deep layers of the developing cerebral neocortex. Fluorescence images of the coronal sections of the primary somatosensory cortex from neonatal mice. (*A*) The first frame of NO imaging (0 s). Squares 1a–e (region 1) are in upper layers and 2a–e (region 2) are in deep layers of the cerebral neocortex. (*B*) The last frame of NO imaging after stimulation of NMDA (600 s). (*C*) The graph indicates time course of fluorescence intensity at the two regions. Administration of 100 μM NMDA is indicated as a bar on the graph from 90 to 180 s. (*D*) The graph shows variation of fluorescence intensity at each time window in (*C*). Difference in the elevation of fluorescence signal between the upper and the deep layer was noted from 90 to 300 s ($P < 0.001$). Scale bar: 100 μm

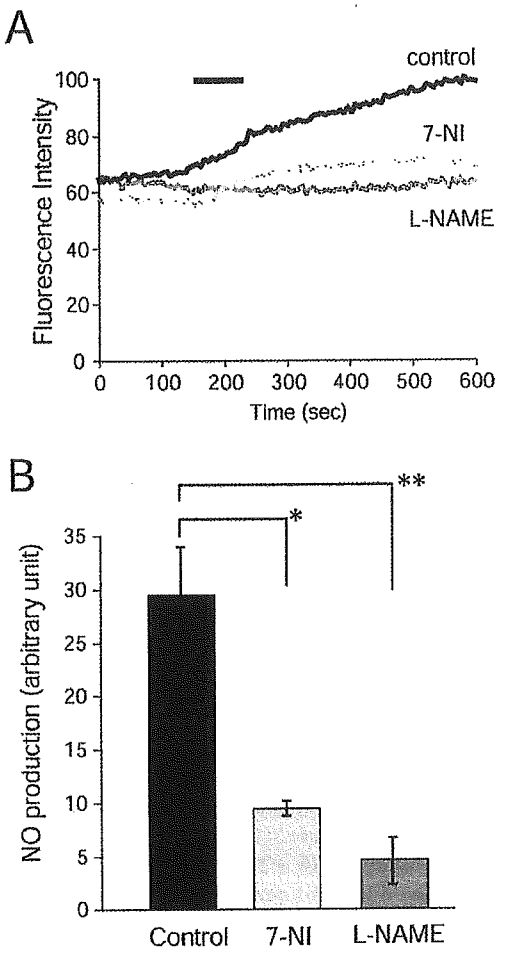

Figure 3. The production of NO in deep layers of the developing cerebral neocortex suppressed by universal NOS inhibitor (L-NAME) or nNOS specific inhibitor (7-NI). (*A*) The graphs indicates time course of fluorescence intensity at the deep layers. Administration of 100 μM NMDA is indicated as a bar on the graph from 150 to 240 s. Each inhibitor was applied to slices for 30 min before the beginning of NO imaging. (*B*) The graph indicates the degree of NO production in deep layers. NO production (arbitrary unit) = (fluorescence intensity at the end [600 s] of the imaging) − (background fluorescence intensity at time 0). Slices treated with 7-NI (9.1 ± 1.1, $n = 3$, mean ± SEM) or L-NAME (4.5 ± 2.1, $n = 3$, mean ± SEM) showed a significant decrease in NO production compared with untreated slices (29.6 ± 4.2, $n = 3$, mean ± SEM) (*$P < 0.001$, **$P < 0.001$). Statistical significance: according to paired *t*-test.

which blocks the over-phosphorylation of nNOS (Leamey *et al.*, 2003). (ii) It is possible that there is a Ca^{2+}-independent production of NO at the deep cortical layers in response to NMDA. (iii) A simple explanation might be that there are more NOS-containing processes in the deeper layers, many of which extend long distances away from the NOS somata.

We further evaluated the extent to which NO was produced only in the deep cortical layers of the developing somatosensory cortex. In all experiments, NO production in the upper layers was less than in deep layers, although calcium influx in the upper layers was more prominent than in the deep layers (Fig. 5). The calcium response in the deep layers (arbitrary unit: 20.6 ± 2.27, $n = 21$, mean ± SEM) corresponded to 47.2% of that in the upper layers (43.6 ± 4.89, $n = 21$, mean ± SEM) (Fig. 5*A*). In contrast, NO production in the upper layers (2.62 ± 0.49, $n = 25$, mean ± SEM) was only 14.6% of that in the deep layers (17.9 ± 0.91, $n = 25$, mean ± SEM) (Fig. 5*B*). Therefore, the conclusion can be drawn that the production of NO was limited to the deep layers of developing cortical plates.

Layer-specificity of NO Production in Developing Somatosensory Cortex

In order to examine whether the production of NO is restricted to specific layers in cortical plates of P0 mice, we performed NO imaging in combination with Toluidine Blue staining after resectioning of imaged slices (Fig. 6*A–C*). In this analysis, we can identify each cortical layer from the size, density and morphology of neurons visualized with Toluidine Blue staining. As described above, NO production after NMDA application was

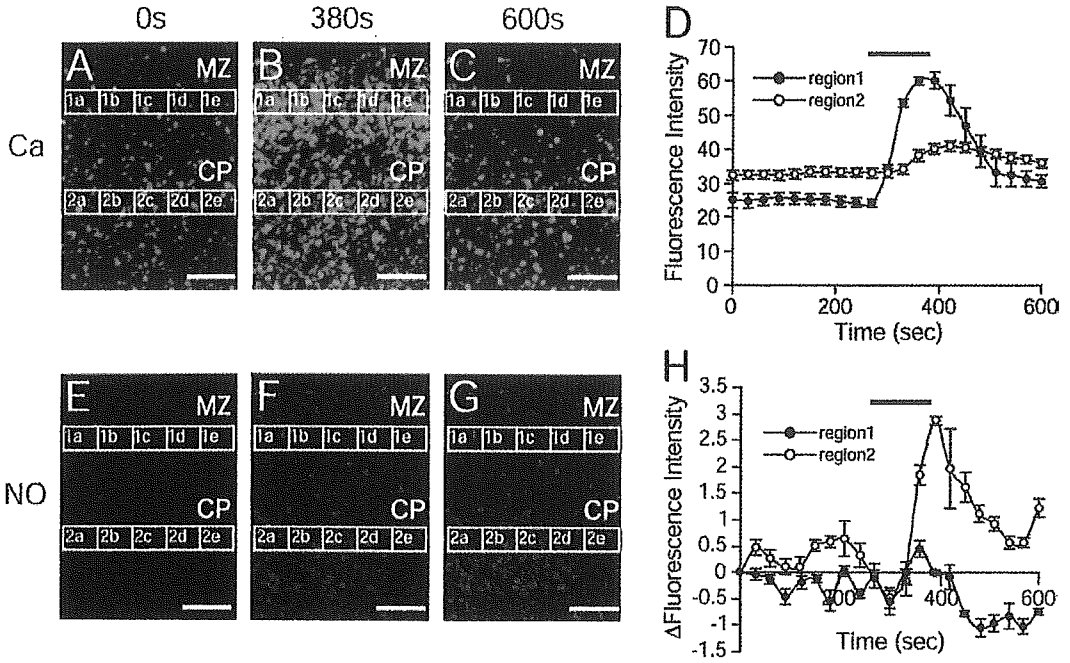

Figure 4. NO-Ca^{2+} dual imaging in the primary somatosensory cortex. (*A–C*) Fluorescence images for Ca^{2+} detection using fluo-4. (*E–G*) Fluorescence images for NO detection using DAR-4M. (*A, E*) Fluorescence images taken 5 min prior to NMDA application (0 s). (*B, F*) Fluorescence images 120 s after onset of NMDA application. (*C, G*) Fluorescence images 600 s after recording of first frames (in *A, E*). (*D, H*) Time course of calcium influx and NO production as calculated from the fluorescence intensity of regions 1 and 2 respectively (see Materials and Methods for calculation used in producing each point). Application of 100 μM NMDA is indicated as a bar in the upper part of the graph from 260 to 380 s. Scale bar in fluorescence images: 80 μm

located in layers V and VI of the developing cortical plate at P0 (Fig. 6*A,B*)—these are the layers of the somatosensory cortex in P0 brains where transient synapses are formed (Higashi *et al.* 2002). Next, we compared the degree of NO production among the layers of somatosensory cortex of P0 mice brain (Fig. 6*D*). In P0 mice, the increase in fluorescence in layer V (52.4 ± 7.62, $n = 7$, mean ± SEM) and VI (36.8 ± 12.8, $n = 7$, mean ± SEM) was detected more strongly than that in upper layers II–IV (11.9 ± 5.62, $n = 7$, mean ± SEM) and MZ (9.23 ± 3.35, $n = 7$, mean ± SEM). At this stage, a boundary of NO production between layer IV and layer V can be distinguished.

We subsequently analyzed the layer-specific production of NO using fresh cortical slices from later developmental stages. NO production in the developing cortical plate of P10 mice was evaluated by NO imaging, and the layer-specificity of NO production was evaluated by Toluidine Blue staining after resectioning imaged slices (Fig. 7). The limit of NO production was shifted to layer IV, where thalamocortical axons reach and form branches and synapses (Fig. 7*A–C*). To assess the relationship between NO production and nNOS expression, furthermore, we performed immunohistochemistry for nNOS protein and NADPH-d histochemistry with resectioned slices (Fig. 7*D,E*). The two types of nNOS expressions were observed at the P10 stage (Fig. 7*D,E*), as well as the P0 stage. Neurons that were strongly positive for both nNOS and NADPH-d were observed and were evenly distributed throughout cortical layers; however, we did not detect any NO production from such a neuron that strongly expressed nNOS. The other type reflects a light and diffuse nNOS expression, which was distributed evenly across layers II–VI. A NO imaging study showed that nNOS proteins expressed lightly at layer IV–VI produce NO, while nNOS in neurons from layer II/III produces only a limited amount of

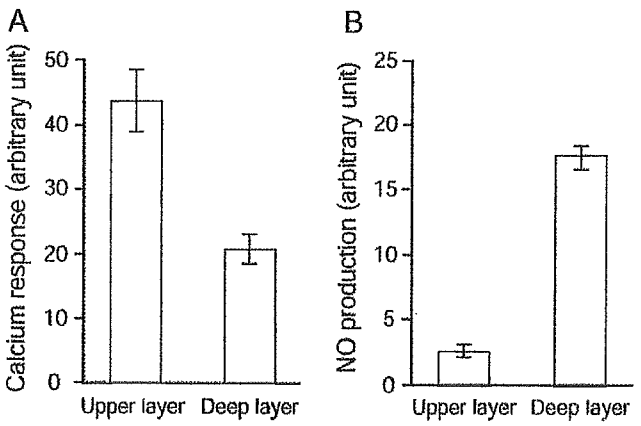

Figure 5. Layer-specific pattern of NO production is opposite to that of calcium influx at P0. Layer-specific response of calcium influx and NO production was compared between the two cortical areas (upper layers versus deep layers). (*A*) The graph indicates the relative degree of peak calcium response after NMDA stimulation at each region. Calcium response (arbitrary units) = (fluorescence intensity at the peak of calcium response) − (background fluorescence intensity at time 0). The mean ± SEM ($n = 25$) are shown. Statistical significance between the two regions is $P < 0.05$ according to paired *t*-test. (*B*) The graph indicates the degree of NO production in each region. NO production (arbitrary unit) = (fluorescence intensity at the end of the imaging) − (background fluorescence intensity at time 0). The mean ± SEM ($n = 25$) are shown. Statistical significance: $P < 0.001$ according to paired *t*-test.

NO. We evaluated the amount of NO production among layers of somatosensory cortex of P10 mice brain (Fig. 7*F*). In P10 mice, the increases in fluorescent signal at layers IV (88.4 ± 12.7, $n = 4$, mean ± SEM) and V (79.5 ± 10.1, $n = 4$, mean ± SEM) and VI (88.2 ± 10.7, $n = 4$, mean ± SEM) were higher than that in layers II/III (18.8 ± 9.92, $n = 4$, mean ± SEM) and MZ (8.8 ± 6.15, $n = 4$,

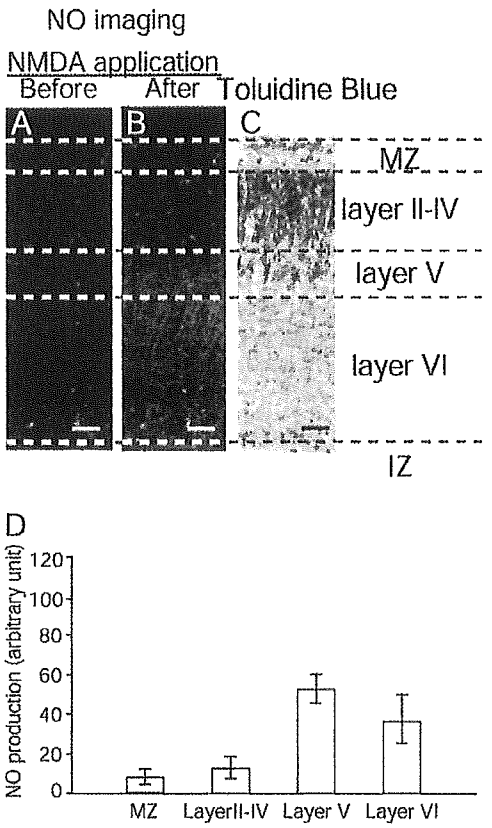

Figure 6. NO production restricted to layers V and VI at somatosensory cortex of P0 mouse. (*A*) Fluorescence images of NO imaging slice before the application of 100 μM of NMDA for 90 s. (*B*) Fluorescence images of NO imaging slice after the application of 100 μM of NMDA for 90 s. (*C*) Toluidine Blue-stained image of resectioned slice of NO imaging slice. Scale bar: 50 μm. (*D*) The graph indicates the degree of NO production in each layer. The mean ± SEM ($n = 8$) are shown. Note: statistical significance between layer IV and layer V was $P < 0.05$ according to paired *t*-test (see Fig. 2 legend).

mean ± SEM). This pattern of NO production may reflect the occurrence of layer-specific circuit formation in the developing neocortex (Molnar *et al.*, 2000; Lopez-Bendito and Molnar, 2003).

To assess the relationship between NO production and barrel formation in layer IV of P10 somatosensory cortex, we performed NO imaging with tangential brain slices containing barrel structure in layer IV. We observed elevated fluorescence intensity in layer IV with the shape of barrel (Fig. 8*A*), which was confirmed by CO staining using imaged slices (Fig. 8*B*). In addition, in order to evaluate whether NO detected in layer IV corresponds to neuronal cell bodies in layer IV, we performed single-cell imaging using cortical slices of P10 mice (Fig. 9). After a cortical cell was identified as a neuron by its spontaneous synaptic current, we recorded this neuron with glass pipette and evaluated its NO production (Fig. 9*A,E*). After NMDA application, inward NMDA-activated current was observed in this neuron of layer IV (Fig. 9*B*), and then the elevation of NO-related fluorescence signals was evaluated at the exact cell simultaneously (Fig. 9*B,C*). As the time-resolution in this NO imaging is 1.09 s, it can be shown that this layer IV neuron produced NO for 1 s after NMDA stimulation (Fig. 9*C*).

In order to examine whether NO is still produced in cortical plates of young adult (P30) mice, we performed NO imaging in combination with Toluidine Blue staining (Fig. 10*A–C*). Weak NO production after NMDA application was observed uniformly in layers II–VI of the developing cortical plate (Fig. 10); however, the degree of NO production is significantly lower than that in P10 as well as P0 cortical plates. Taken together, these results indicate that layer-specific NO production which may affect layer-specific cortical circuit formation is terminated at young adult stage P30.

Discussion

In this study, we demonstrate for the first time the real-time detection of NO production in the cortical plate of the neonatal

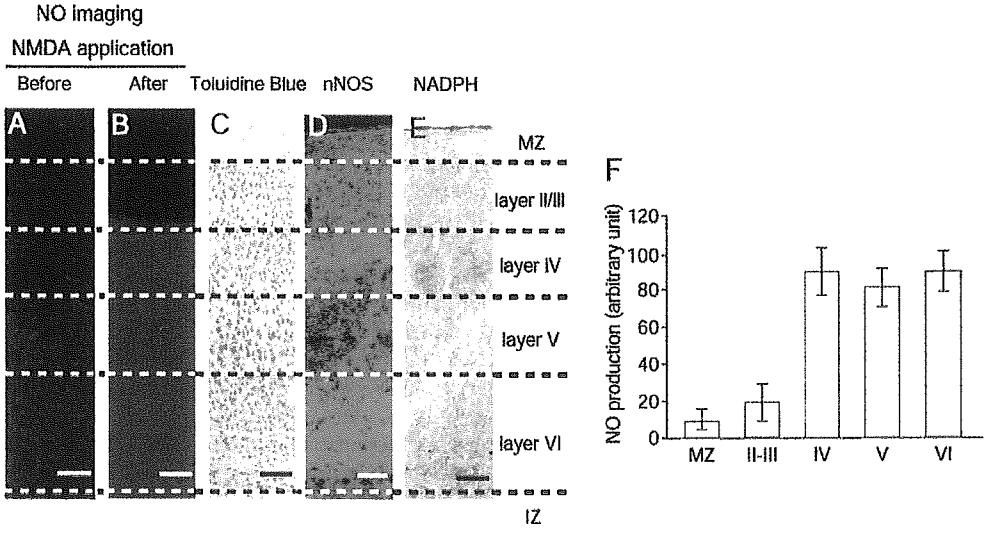

Figure 7. NO production expanded to layer IV of somatosensory cortex at P10 mouse. (*A*) Fluorescence images of NO imaging slice with consecutive scans along the *z*-axis before the application of 100 μM of NMDA for 90 s. (*B*) Fluorescence images of NO imaging slice with consecutive scans along the *z*-axis after the application of 100 μM of NMDA for 90 s. (*C*) Toluidine Blue-stained image of resectioned slice of NO imaging slice. (*D*) nNOS-stained image of resectioned slice of NO imaging slice. (*E*) NADPH-diaphorase histochemical image of resectioned slice of NO imaging slice. Scale bar: 100 μm. (*F*) The graph showing the difference in NO production between cortical layers at somatosensory cortex of P10 mouse. The histogram indicates the degree of NO production in each layer. The mean ± SEM ($n = 4$) are shown. Note: statistical significance between layer II/III and layer IV were $P < 0.01$ according to paired *t*-test.

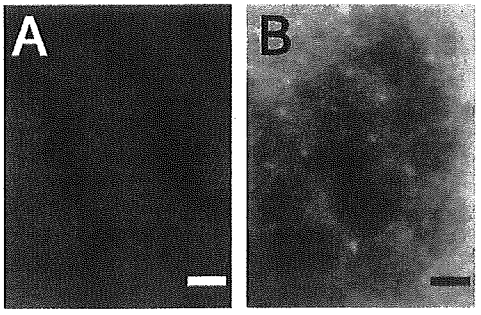

Figure 8. NO imaging using P10 tangential slices. (*A*) After the stimulation of NMDA, DAR-4M loaded cortical slice was sequentially visualized with 10× lens, and a combined image from a numbers of NO imaging flames is shown. (*B*) Cytochrome oxidase staining using the imaged slice. Similar results were obtained from other two experiments. Scale bar: 200 μm.

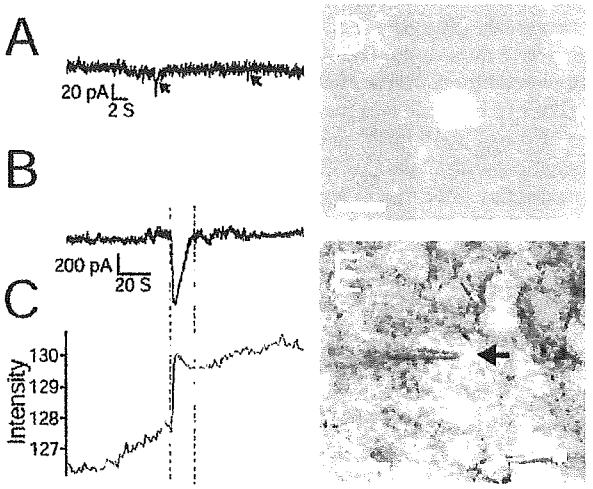

Figure 9. NO production in a neuron in layer IV of cerebral cortex of P10 mice. (*A*) Spontaneous synaptic current indicating neuron from a recorded cell (arrows), data (*B–E*) were obtained from the same neuron. (*B*) Current response to NMDA after focal administration. (*C*) NO production after focal administration of NMDA. The fluorescence images were obtained sequentially at intervals of 1.09 s. (*D*) Fluorescence image with DAR4M. (*E*) Infrared DIC image. NMDA was applied focally to the recording and imaged cell (arrow) via a glass pipette (asterisk). Similar results were obtained from three other layer IV neurons. Scale bar: 10 μm.

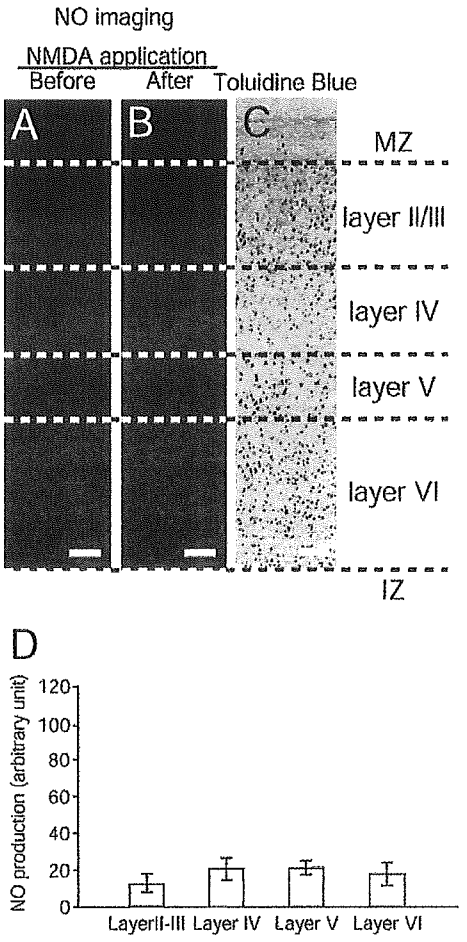

Figure 10. Weak NO production spread throughout cortical plates in P30 mouse. (*A*) Fluorescence images from the NO imaging study with consecutive scans along the *z*-axis before the application of 100 μM of NMDA for 90 s. (*B*) Fluorescence images of NO imaging slice with consecutive scans along the *z*-axis after the application of 100 μM of NMDA for 90 s. (*C*) Toluidine Blue-stained image of resectioned slice of NO imaging slice. Scale bar: 100 μm. (*D*) The graph indicates the degree of NO production in each layer. The mean ± SEM ($n = 4$) are shown

mouse brain. We have shown that the production sites of NO in the somatosensory cortex of newborn pups (P0 mice) just after stimulation with NMDA were located in the deep cortical layers (layers V and VI) where transient synapses are formed (Higashi *et al.* 2002), but not in the upper cortical layers (layers II–IV). As cortical development proceeds, NO production sites spread to layer IV, where thalamocortical axons preferentially make connections with cortical neurons (Higashi *et al.*, 1999; Lopez-Bendito and Molnar 2003). At P30, layer-specific NO production was not detected. Taken together, these results strongly suggest that NO plays an important role in the formation of cortical neuronal networks.

In the present study, we evaluated which type of NOS distribution actively releases NO upon NMDA stimulation. In the developmental stage of the cerebral cortex, a series of reports have suggested a lamina-specific pattern of NADPH-diaphorase activity (Wong-Riley *et al.*, 1998; Vercelli *et al.*, 1999), which would probably reflect NOS activity (Bredt *et al.*, 1991; Dawson *et al.*, 1991). In particular, Vercelli *et al.* (1999) have carefully analyzed the distribution of NADPH-d staining during rat cortical development (E17–P21) and proposed four types of distribution. (i) A transient and diffuse neuropil staining that is visible in deep layers before birth and then segregates into whisker-specific patches in layer IV until P15. An intense staining of (ii) scattered cells and of (iii) a plexus of fibers distributed in all layers. (iv) Light staining of cortical neurons detected mostly in layers II–IV. We have clearly demonstrated lamina-specific production of NO, which was observed in deep layers at birth and then spreads to layer IV up to P10. This pattern is quite similar to the transient and diffuse neuropil staining obtained by Vercelli *et al.* (1999). At this stage, several candidates for the site for NO production can be postulated, but the actual release of NO should be limited from NOS molecules, which aredistributed in a transient and diffuse neuropil pattern. Although, in general, NMDA-R channels are blocked by magnesium in a voltage-dependent manner, NMDA-R channels at the early postnatal stage could be activated via the $GABA_AR$ and GlyR systems (Ben-Ari *et al.*, 1989; Owens *et al.*, 1996; Miyakawa *et al.*, 2002). It could be postulated that NO production by such